Adipokinetic hormone signaling mediates the enhanced fecundity of *Diaphorina citri* infected by '*Candidatus* Liberibacter asiaticus'

Jiayun Li[1], Paul Holford[3], George Andrew Charles Beattie[3], Shujie Wu[1], Jielan He[1], Shijian Tan[1], Desen Wang[1], Yurong He[1], Yijing Cen[1]*, Xiaoge Nian[1,2]*

[1]National Key Laboratory of Green Pesticide, Department of Entomology, College of Plant Protection, South China Agricultural University, Guangzhou, 510642, China；

[2]Henry Fok School of Biology and Agriculture, Shaoguan University, Shaoguan, 512005, China；

[3]School of Science, Western Sydney University, Locked Bag 1797, Penrith, NSW 2751, Australia;

*Corresponding author: Yijing Cen and Xiaoge Nian

Email: cenyj@scau.edu.cn; nianxiaoge@scau.edu.cn

Abstract

Diaphorina citri serves as the primary vector for '*Candidatus* Liberibacter asiaticus' (*C*Las), the bacterium associated with the severe Asian form of huanglongbing. *C*Las-positive *D. citri* are more fecund than their *C*Las-negative counterparts and require extra energy expenditure. Therefore, understanding the molecular mechanisms linking metabolism and reproduction is of particular importance. In this study, we found adipokinetic hormone (*DcAKH*) and its receptor (*DcAKHR*) were essential for increasing lipid metabolism and fecundity in response to *C*Las infection in *D. citri.* Knockdown of *DcAKH* and *DcAKHR* not only resulted in the accumulation of triacylglycerol and a decline of glycogen, but also significantly decreased fecundity and *C*Las titer in ovaries. Combined *in vivo* and *in vitro* experiments showed that miR-34 suppresses *DcAKHR* expression by binding to its 3' untranslated region, whilst overexpression of miR-34 resulted in a decline of *DcAKHR* expression and *C*Las titer in ovaries and caused defects that mimicked *DcAKHR* knockdown phenotypes. Additionally, knockdown of *DcAKH* and *DcAKHR* significantly reduced juvenile hormone (JH) titer and JH signaling pathway genes in fat bodies and ovaries, including the JH receptor, *methoprene-tolerant* (*DcMet*), and the transcription factor, *Krüppel homolog 1 (DcKr-h1)*, that acts downstream of it, as well as the egg development related genes *vitellogenin 1-like* (*DcVg-1-like*), *vitellogenin A1-like* (*DcVg-A1-like*) and the vitellogenin receptor (*DcVgR*). As a result, *C*Las hijacks AKH/AKHR-miR-34-JH signaling to improve *D. citri* lipid metabolism and fecundity, while simultaneously increasing the replication of *C*Las, suggesting a mutualistic interaction between *C*Las and *D. citri* ovaries.

Key words: huanglongbing; *Diaphorina citri*; *DcAKH*/*DcAKHR*; miR-34; mutualism

Introduction

The majority of devastating plant pathogens, including viruses and bacteria, are transmitted by insect vectors [1]. In recent decades, the interactions between vectors and pathogens have been widely studied [1-4]. However, studies on the mechanisms underlying these interactions have mainly focused on vector-virus or vector-fungus interactions; less research has been performed on vector-bacteria interactions. Knowledge of the relationships between vectors and pathogens is of great significance for understanding the epidemiology of plant pathogens, and this knowledge may help develop new strategies for controlling both vectors and pathogens. The severe Asian form of huanglongbing (HLB) is currently the most destructive citrus disease in Asia and the Americas where it is associated with the phloem-restricted, Gram-negative, α-Proteobacteria '*Candidatus* Liberibacter asiaticus' (*C*Las) and transmitted by the Asian citrus psyllid, *Diaphorina citri* Kuwayama (Hemiptera: Psyllidae) [5-9]. However, since *C*Las has not been cultured *in vitro,* Koch's postulates have not been proven. Control of *D. citri* is the most effective way to prevent HLB epidemics [6,7] but experience in Asia [10] and the United States of America [11,12], and recent press reports from Brazil, indicate that it is impossible to suppress psyllid populations with insecticides to levels that prevent spread of *C*Las.

Previous studies have reported that infection with *C*Las significantly increases the fecundity of *D. citri* [13-15]. Reproduction is a costly process in terms of energy usage in the adult life of female insects [16], and there is an inevitable trade-off between lipid storage and use, because animals mobilize their lipid reserves during reproduction. However, the mechanism of how *D. citri* maintains a balance between lipid metabolism and increased fecundity after infection with *C*Las remains unknown. In insects, energy mobilization is under control of adipokinetic hormone (AKH), which was the first insect neurohormone to be identified; it was shown to stimulate lipid mobilization for locomotor activity in locusts [17]. To date, more than 80 different forms of AKH have been identified or predicted in arthropod species due to similar structural characteristics of the enzyme [18]. The mechanisms of synthesis and biological activity of AKH have also been investigated. Insect store lipids in the form of triacylglycerides (TAG) and as carbohydrates in the form of glycogen in their fat bodies [19]. Under conditions of energy demand, AKHs are synthesized in the corpora cardiaca,

69 released into the hemolymph and bind to receptors (AKHRs) located on the plasma membrane
70 of fat body cells. AKHR binding and activation triggers the release of energy-rich substrates
71 after which various cellular signaling pathway components come into play [20]. AKHRs are a
72 class of G protein-coupled receptors and were first identified in *Drosophila melanogaster* [21]
73 and *Bombyx mori* [22]; subsequently, they were identified in a large number of insect species
74 [23-26].

75 While the AKH pathway is recognized for its role in mobilizing stored lipids, its involvement
76 in vector-pathogen interactions remains understudied. For example, in *Anopheles*
77 *gambiae-Plasmodium falciparum* interactions. *P. falciparum* infection influences *A. gambiae*
78 AKH signaling, lipid metabolism, and mobilization of energy reserves to support the parasite's
79 metabolic and structural needs [27]. In another example, infection of cockroaches with the
80 fungus *Isaria fumosorosea* result in a significant rise in AKH levels in the central nervous
81 system in response to stress responses [28]. The functions of the AKH/AKHR in
82 insect-pathogen interactions need further investigation. Recent studies have shown that
83 AKH/AKHR signaling plays a regulatory role during female reproduction in insects. For
84 example, depletion of AKHR in *Bactrocera dorsalis* resulted in TAG accumulation, decreased
85 sexual courtship activity, and fecundity [29]. AKHR knockdown in *Nilaparvata lugens* interferes
86 with trehalose homeostasis and vitellogenin uptake by oocytes, which causes delayed oocyte
87 development and reduced fecundity [30]. AKH/AKHR signaling also regulates vitellogenesis
88 and egg development in *Locusta migratoria* via triacylglycerol mobilization and trehalose
89 homeostasis [31]. As outlined above, the fecundity of *D. citri* is increased by *C*Las. Whether
90 AKH/AKHR signaling participates in this increase in fecundity due to infection via alterations in
91 lipid metabolism is not currently known.

92 Although numerous studies have been conducted on the AKH/AKHR signaling pathway,
93 miRNA-mediated regulation of the AKH signaling pathway at the post-transcriptional level has
94 been little studied. MicroRNAs (miRNAs) are small, non-coding RNAs containing
95 approximately 22 nucleotides that act mostly on the 3' untranslated region (UTR) of target
96 mRNAs, resulting in translation repression or mRNA degradation [32]. miRNAs play important
97 roles in regulating cellular events at the post-transcriptional level during biological processes
98 [32,33,34]. For example, in *D. citri-C*Las interaction, *C*Las hijacks the JH signaling pathway

99 and host miR-275 that targets the *vitellogenin receptor* (*DcVgR*) to improve *D. citri* fecundity,
100 while simultaneously increasing the replication of *C*Las itself, suggesting a mutualistic
101 interaction in *D. citri* ovaries with *C*Las [35]. In term of host-virus interactions, miR-8 and
102 miR-429 target *Broad isoform Z2*, the gene involved in the hormonal regulation of single
103 nucleopolyhedrovirus (HaSNPV)-mediated climbing behavior in *Helicoverpa armigera* [36]. In
104 relation to reproduction, in *Aedes aegypti*, miR-275 is essential for egg development [37],
105 miR-309 for ovarian development [38] and miR-8 for other reproductive processes [39]. As for
106 lipid metabolism, knockdown of miR-277 in *A. aegypti* activates insulin/FOXO signaling by
107 increasing the expression of ilp7 and ilp8, which reduces TAG levels and inhibits ovarian
108 development [40]. Nevertheless, the functions of the miRNAs in insect-pathogen interactions
109 need further investigation. To date, there are no reports that miRNAs participate in *D.*
110 *citri*-*C*Las interactions or are hijacked by *C*Las to affect lipid metabolism and the fecundity of *D.*
111 *citri*. As a consequence, in this study, we used the *D. citri*-*C*Las system as a model to study the
112 molecular events associated with AKH/AKHR signaling that affect lipid metabolism and
113 increase fecundity of *D. citri* induced by *C*Las. Our study contributes to our understanding of
114 the interactions between vectors and pathogens and may also provide new ways for
115 controlling *D. citri* and HLB.
116

117 ## Results

118 **Effects of *C*Las infection on the reproduction and metabolism of adult *D. citri*.**

119 Total TAG and glycogen levels in fat bodies of *C*Las-negative and *C*Las-positive psyllids
120 were determined. After infection with *C*Las, the TAG and glycogen levels of *C*Las-positive
121 psyllids significantly increased compared with *C*Las-negative individuals (Figures 1A-B). Since
122 TAG is mainly stored in fat bodies as lipid droplets, we next evaluated the changes in the lipid
123 droplet size using Nile red staining. As shown in Figure 1C, the size of lipid droplets in the
124 *C*Las-positive group was significantly larger than those of the *C*Las-negative group. In order to
125 evaluate the effects of *C*Las on the reproduction of *D. citri*, the preoviposition period,
126 oviposition period and fecundity of both *C*Las-negative and *C*Las-positive psyllids were
127 examined. After infection with *C*Las, the preoviposition period was significantly shortened, the
128 oviposition period was extended, and the fecundity was markedly increased (Figures 1D-E).

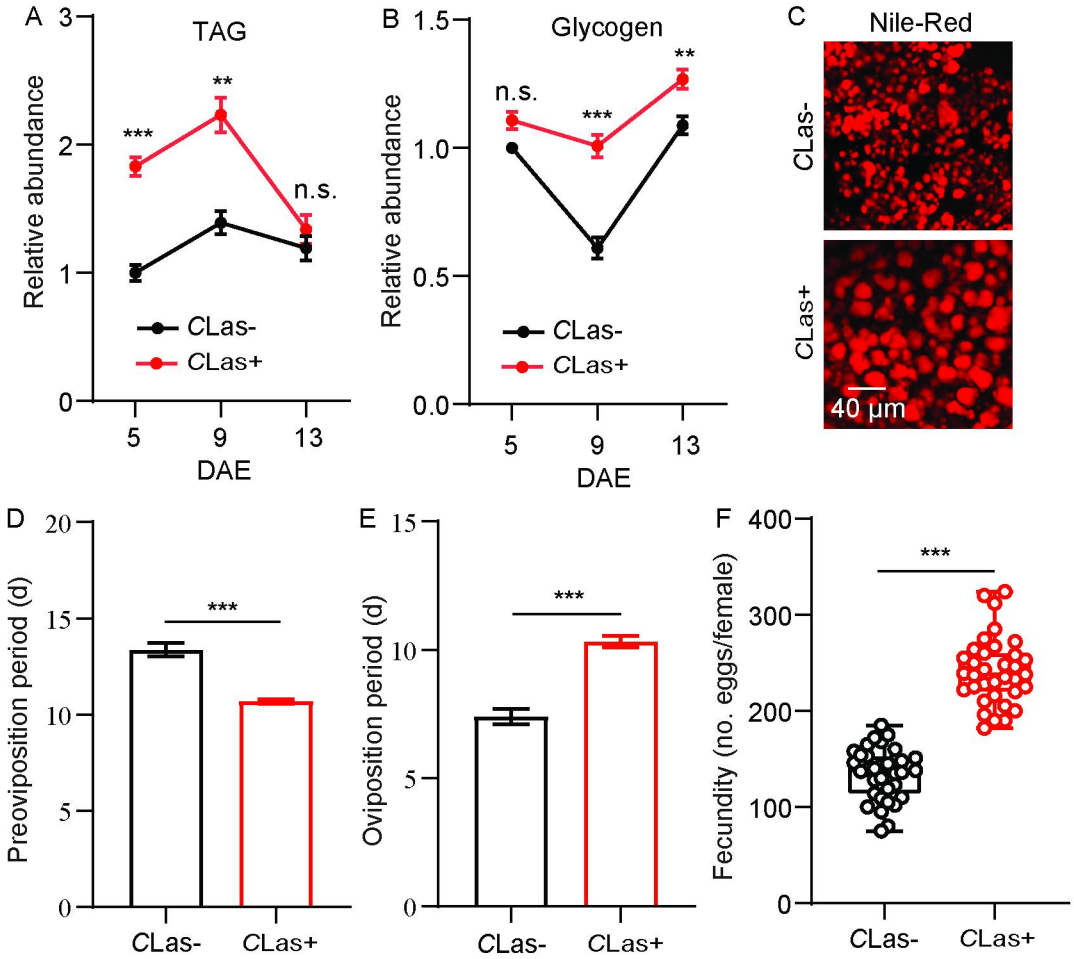

129

130 **Figure 1. Effects of *C*Las on lipid metabolism and reproductive behavior of *D. citri*.**

131 (A) Comparison of TAG levels in the fat bodies of *C*Las-positive (*C*Las+) and *C*Las-negative

132 (*C*Las-) females 5, 9, 13 days after emergence (DAE). (B) Comparison of glycogen levels in
133 the fat bodies of *C*Las+ and *C*Las- females 5, 9, 13 DAE. (C) Lipid droplets in fat bodies
134 dissected from *C*Las+ and *C*Las- females 9 DAE stained with Nile red. Scale bar = 40 μm.
135 (D-F) Comparison of the preoviposition period, oviposition period and the fecundity of *C*Las+
136 and *C*Las- adults. Data are shown as means ± SEM. The significant differences between
137 *C*Las-positive and *C*Las-negative psyllids were determined using Student's *t*-tests (**$p < 0.01$,
138 ***$p < 0.001$).
139
140 ***DcAKH* is involved in changes in metabolism and fecundity in *D. citri* mediated by *C*Las**
141 Using our transcriptome database, cDNA sequences of *DcAKH* were identified and
142 cloned. The cDNA sequence of *DcAKH* is 225 bp in length, encodes a deduced polypeptide of
143 74 amino acid residues and has the conserved structural characteristics of a neuropeptide.
144 The conserved structure was "signal peptide + mature peptide + related peptide", and the
145 mature peptide sequence of *Dc*AKH is "QVNFSPNW" (Figure S1A). A phylogenetic analysis
146 was conducted to evaluate the association of *Dc*AKH with other insect AKHs; *Dc*AKH was
147 most closely related to the AKHs of three hemipteran species, *Nilaparvata lugens*, *Sitobion*
148 *avenae* and *Acyrthosiphon pisum* (Figure S1B).
149 Tissue expression profiles showed that *Dc*AKH was expressed at the highest level in the
150 brain, significantly higher than in the ovaries, fat bodies, and midgut in *D. citri* (Figure S2). The
151 levels of *DcAKH* in ovaries of *C*Las-negative and -positive psyllids decreased during the
152 assessment period. However, levels in the ovaries of *C*Las-positive psyllids were significantly
153 higher than those that were *C*Las-negative at all assessment times (Figure 2A). To investigate
154 the role of *DcAKH* in metabolic and reproductive changes induced by *C*Las, we knocked down
155 *DcAKH* expression using RNAi. When fed with ds*DcAKH*, the mRNA level of *DcAKH* in
156 *C*Las-negative and *C*Las-positive ovaries significantly decreased by 89% and 66%,
157 respectively, compared with psyllids fed with ds*GFP* (Figure 2B). Knockdown of *DcAKH*
158 resulted in TAG accumulation and a significant decrease in glycogen (Figures 2C-D).
159 Correspondingly, depletion of *DcAKH* led to a significant increase the size of the lipid droplets
160 (Figure 2E). Compared with the controls, *DcAKH* RNAi slowed ovarian development (Figure
161 2F), extended the preoviposition period (from 13.3 to 14.2 days in *C*Las-negative psyllids and

162 from 10.7 to 13.4 days in *C*Las-positive psyllids), shortened the oviposition period (from 7.1 to
163 4.3 days in *C*Las-negative psyllids and from 10.1 to 5.7 days in *C*Las-positive psyllids), and
164 decreased fecundity (from 138.0 to 94.7 days in *C*Las-negative psyllids and from 230.0 to
165 118.1 days in *C*Las-positive psyllids) (Figures 2G-I). Furthermore, the *C*Las signal and relative
166 titer in the ovaries of *DcAKH* knockdown psyllids significantly decreased (Figures 2J-K). Taken
167 together, it can be concluded that *DcAKH* is involved in *C*Las-induced metabolic and
168 reproductive changes in *D.citri.*

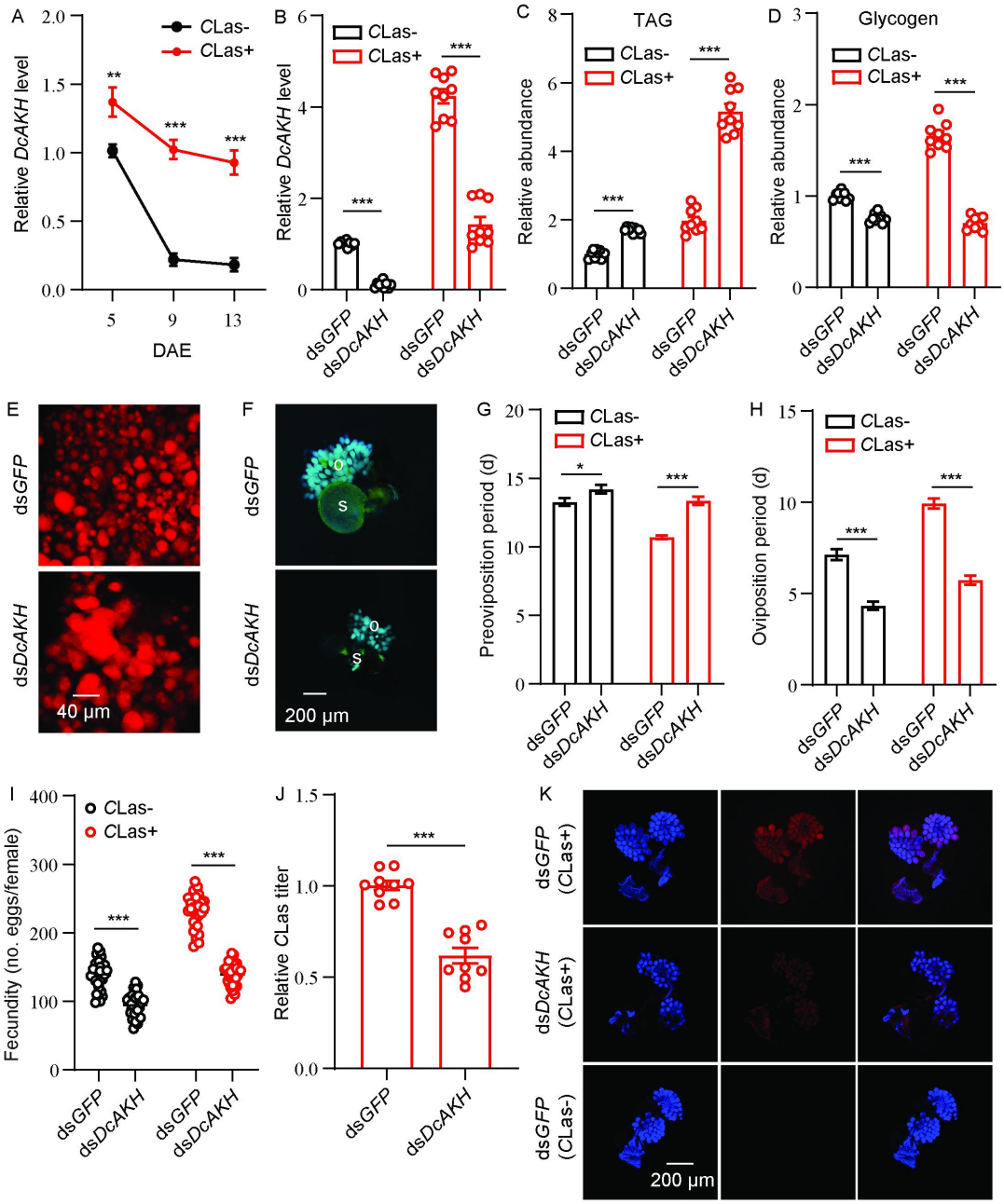

Figure 2. *DcAKH* is involved in the mutualistic relationship between *C*Las and *D. citri* resulting in increased fecundity. (A) Comparison of temporal expression patterns of *DcAKH* between the ovaries of *C*Las- and *C*Las+ psyllids. (B) Efficiency of RNAi of *DcAKH* in *C*Las- and *C*Las+ females treated with ds*DcAKH* for 48 h. (C) Comparison of TAG levels in fat bodies of *C*Las- and *C*Las+ females treated with ds*DcAKH* for 48 h. (D) Comparison of glycogen levels in fat bodies of *C*Las- and *C*Las+ females treated with ds*DcAKH* for 48 h. (E) Lipid droplets stained with Nile red in fat bodies dissected from *C*Las+ females treated with ds*DcAKH* for 48 h. Scale bar = 40 μm. (F) Ovary phenotypes of *C*Las+ females treated with

178 ds*DcAKH* for 48 h. Scale bar = 200 μm. o: ovary, s: spermathecae. (G-I) Comparison of the
179 preoviposition period, oviposition period and the fecundity between *C*Las- and *C*Las+ adults
180 treated with ds*DcAKH*. (J) The *C*Las titer in ovaries of *C*Las+ females treated with ds*DcAKH*
181 for 48 h. (K) Representative confocal images of *C*Las in the reproductive system of *C*Las+
182 females treated with ds*DcAKH* for 48 h. Scale bar = 200 μm. DAPI: the cell nuclei were stained
183 with DAPI and visualized in blue. *C*Las-Cy3: the *C*Las signal visualized in red by staining with
184 Cy3. Merge: merged imaging of co-localization of cell nuclei and *C*Las. Data are shown as
185 means ± SEM. The significant differences between treatment and controls are indicated by
186 asterisks (Student's *t*-test, $*p < 0.05$, $**p < 0.01$, $***p < 0.001$).
187
188 ***DcAKHR* respond to *DcAKH* and participates in *D. citri*-CLas mutualism**
189 The protein tertiary structure of *DcAKHR* was predicted; *DcAKHR* has seven conserved
190 transmembrane (TM1-TM7) domains and is a typical G protein coupled receptor (Figure S3A).
191 A phylogenetic analysis was conducted to evaluate the association of *DcAKHR* with other
192 insect *AKHRs*; *DcAKHR* was most closely related to the *AKHR* of *Nilaparvata lugens* (Figure
193 S3B). To further confirm *Dc*AKH can activate *DcAKHR*, we performed a cell-based calcium
194 mobilization assay. As shown in Figure S3C, *DcAKHR* was strongly activated by *Dc*AKH in a
195 dose-dependent manner, with an EC_{50} value of 2.20×10^{-5} mM, but there were no responses
196 when challenged with an empty vector or other evolutionarily-related peptides. In addition,
197 after *DcAKH* knockdown, *DcAKHR* expression in the ovaries significantly decreased (Figure
198 S3D). *DcAKHR* was cloned, sequenced, designated and then used for further studies.
199 Sequence analysis showed that *DcAKHR* consisted of an open reading frame (ORF) of 1290
200 bp and a 185 bp 3' UTR. It encodes a putative protein consisting of 429 amino acids with a
201 predicted molecular weight of 48.32 kDa. Tissue expression patterns showed that *DcAKHR*
202 had the highest expression in the midgut, follow by the head, fat bodies, and ovaries (Figure
203 S4). In the ovaries of *C*Las-positive and -negative psyllids, the transcript and protein levels of
204 *DcAKHR* increased over the assessment period with levels of both being higher in
205 *C*Las-positive psyllids than in *C*Las-negative psyllids (Figure 3A). To investigate the role of
206 *DcAKHR* in metabolic and reproductive changes induced by *C*Las, we knocked down
207 *DcAKHR* expression by RNAi. When fed with ds*DcAKHR*, the mRNA levels of *DcAKHR* in the

208 ovaries of *C*Las-negative and *C*Las-positive were significantly decreased by 59.4 and 66.0%,
209 respectively, compared with psyllids fed with ds*GFP*; western blot analysis confirmed that
210 *Dc*AKHR protein levels were also significantly reduced (Figure 3B). Knockdown of *DcAKHR*
211 resulted in TAG accumulation and a significant decrease in glycogen (Figures 3C-D).
212 Correspondingly, depletion of *DcAKHR* led to a significant increase in the size of lipid droplets
213 (Figure 3E). Compared with the controls, *DcAKHR* RNAi interfered with ovarian development
214 (Figure 3F): the preoviposition period was extended (from 13.3 to 16.2 days in *C*Las-negative
215 psyllids and from 10.7 to 12.9 days in *C*Las-positive psyllids); oviposition period was shortened
216 (from 7.1 to 4.6 days in *C*Las-negative psyllids and from 10.1 to 5.3 days in *C*Las-positive
217 psyllids); and fecundity decreased (from 138.0 to 90.6 eggs per female in *C*Las-negative
218 psyllids and from 230.0 to 98.2 eggs per female in *C*Las-positive psyllids). These effects are
219 similar to those caused by *DcAKH* knockdown (Figures 3G-I). Furthermore, the *C*Las signal
220 and relative titer in the ovaries of *DcAKH* knockdown psyllids were significantly decreased
221 (Figures 3J-K). Taken together, *DcAKHR* responds to *DcAKH* and is involved in the
222 *C*Las-induced metabolic and reproductive changes in *D. citri.*
223

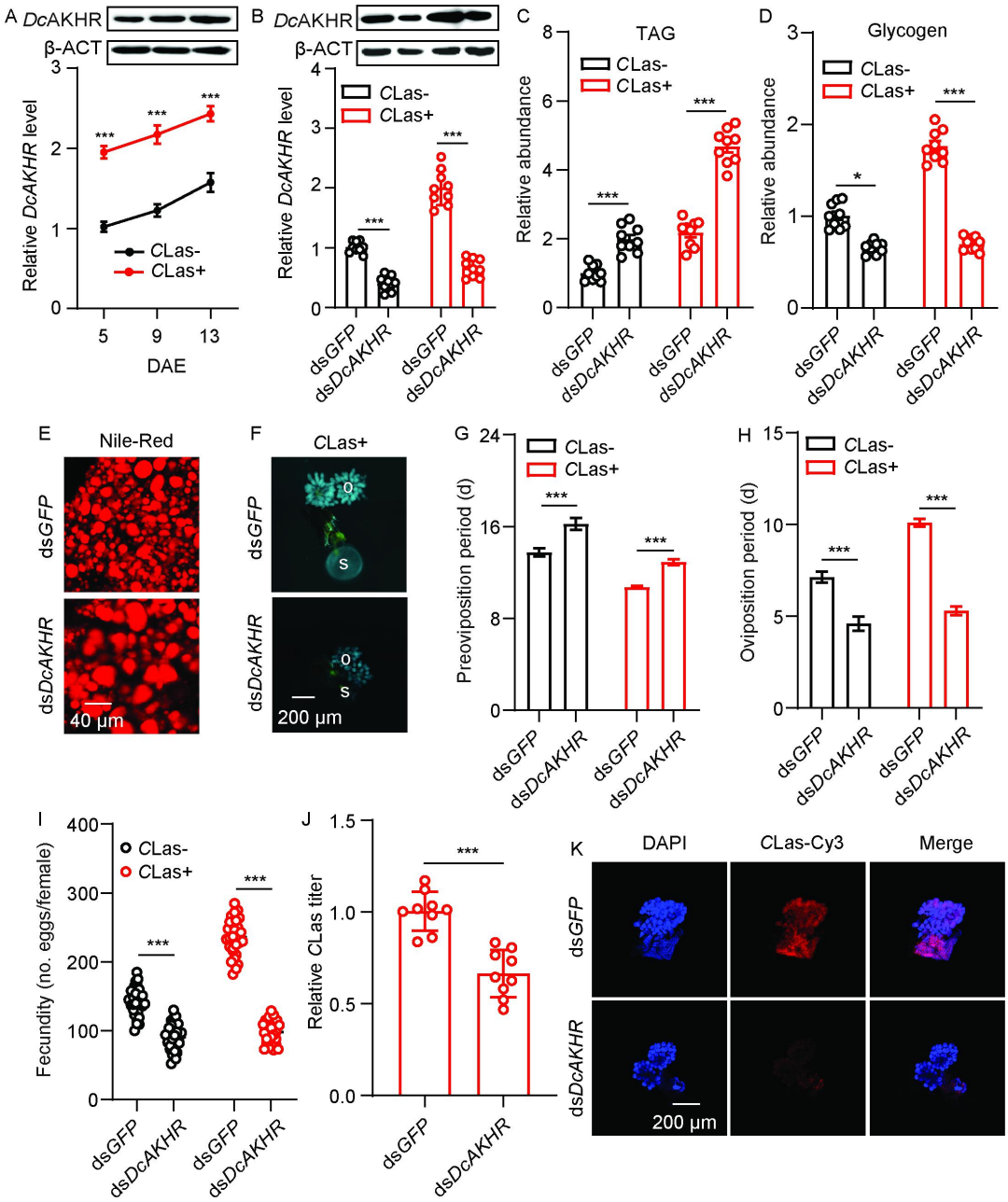

Figure 3. *DcAKHR* is involved in the mutualistic relationship between *C*Las and *D. citri* resulting in increased fecundity. (A) Comparison of temporal expression patterns of *DcAKHR* between the ovaries of *C*Las- and *C*Las+ psyllids. (B) The efficiency of RNAi of *DcAKHR* in *C*Las- and *C*Las+ psyllids treated with ds*DcAKHR* for 48 h. (C) Comparison of TAG levels in fat bodies of *C*Las- and *C*Las+ females treated with ds*DcAKHR* for 48 h. (D) Comparison of glycogen levels in fat bodies of *C*Las- and *C*Las+ females treated with ds*DcAKHR* for 48 h. (E) Lipid droplets stained with Nile red in fat bodies dissected from *C*Las-positive females treated with ds*DcAKHR* for 48 h. Scale bar = 40 μm. (F) Ovary

233 phenotypes of *C*Las+ females treated with ds*DcAKHR* for 48 h. Scale bar = 200 μm. o: ovary,
234 s: spermathecae. (G-I) Comparison of the preoviposition period, oviposition period and the
235 fecundity of *C*Las- and *C*Las+ adults treated with ds*DcAKHR*. (J) The *C*Las titer in the ovaries
236 of *C*Las+ females treated with ds*DcAKHR* for 48 h. (K) Representative confocal images of the
237 reproductive system of *C*Las+ females treated with ds*DcAKHR* for 48 h. Scale bar = 200 μm.
238 DAPI: the cell nuclei were stained with DAPI and visualized in blue. *C*Las-Cy3: the *C*Las signal
239 visualized in red by staining with Cy3. Merge: merged imaging of co-localization of cell nuclei
240 and *C*Las. Data are shown as means ± SEM. The significant differences between treatment
241 and controls are indicated by asterisks (Student's *t*-test, ***$p < 0.001$).
242
243 **miR-34 targeted *DcAKHR***
244 Based on the small RNA libraries of *D. citri*, we used miRanda and RNAhybrid software to
245 predict the potential miRNAs targeting *DcAKHR*; three putative miRNAs, namely miR-34,
246 miR-2 and miR-14 (Figure 4A), were identified. To confirm the binding activity of these
247 miRNAs with *DcAKHR*, several dual-luciferase reporter assays were conducted. Compared
248 with the controls, the luciferase activity was markedly reduced when miR-34 agomir was
249 co-transfected with the recombinant plasmid containing the full 3'UTR sequence of *DcAKHR*,
250 while miR-2 and miR-14 activities were not significantly changed (Figure 4B). In addition, the
251 reporter activity was recovered when the binding sites of miR-34 were mutated in the *DcAKHR*
252 3'-UTR (Figure 4C). To determine whether miR-34 specifically targets *DcAKHR*, the following
253 experiments were conducted. Firstly. tissue expression patterns showed that the miR-34 was
254 highly expressed in the head, followed by the fat bodies, ovaries, and midgut (Figure 4D).
255 Secondly, miR-34 has the opposite expression pattern to *DcAKHR* (Fig. 3A), and transcript
256 levels decreased over the assessment period with the levels of both being lower in
257 *C*Las-positive psyllids than in *C*Las-negative psyllids (Figure 4E). Thirdly, after feeding with
258 agomir-34, the relative levels of miR-34 mRNA in the ovaries of *C*Las-negative and
259 *C*Las-positive psyllids increased 1.9- and 2.3-fold, respectively (Figure S5). The mRNA and
260 protein levels of *DcAKHR* were correspondingly increased or decreased after separately
261 feeding psyllids with either antagomir-34 or agomir-34 (Figure 4F). Fourthly, an RNA
262 immunoprecipitation (RIP) assay was performed; *DcAKHR* mRNA was significantly enriched in

263 the anti-AGO-immunoprecipitated RNAs from ovaries of agomir-34-fed female psyllids relative
264 to the control samples (Figure 4G). Taken together, these results strongly suggest that
265 *DcAKHR* is a direct target of miR-34.

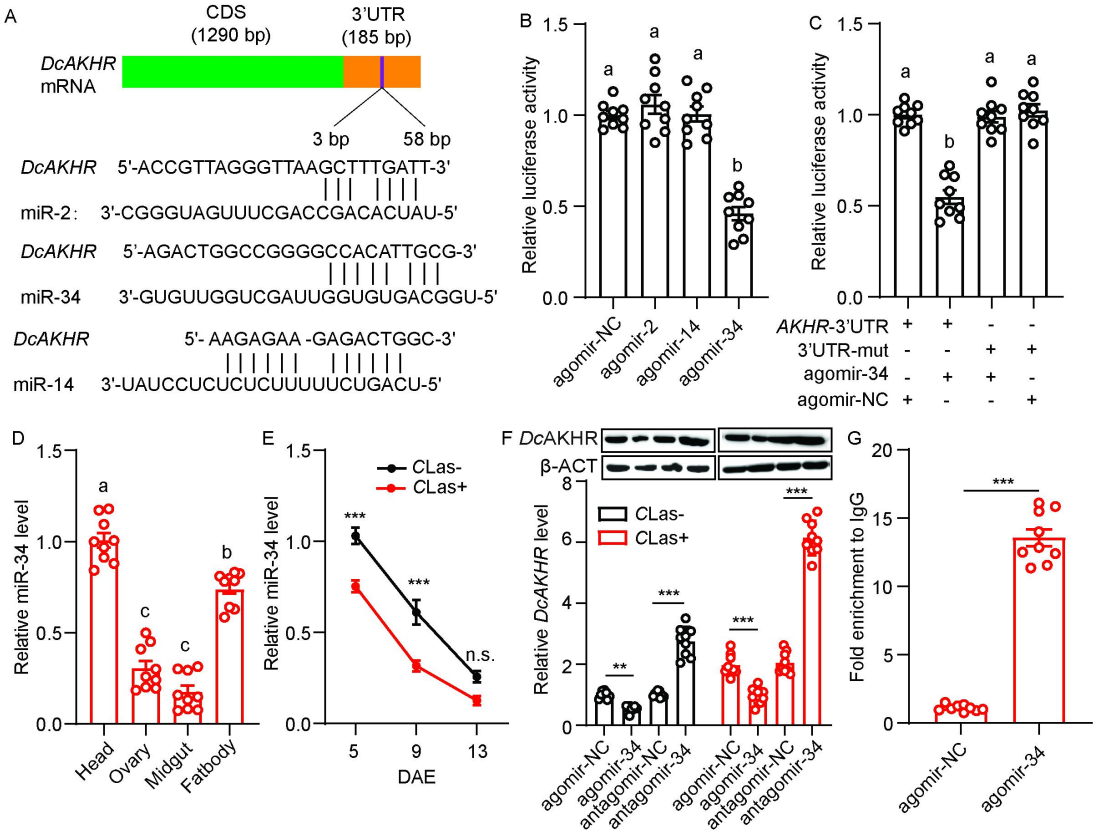

266

267 **Figure 4. Identification and validation of the target relationship between miR-34 and**
268 ***DcAKHR.*** (A) The putative binding sites of miRNAs in the *DcAKHR* 3'-UTR as predicted by
269 miRanda and RNAhybrid. (B) Dual-luciferase reporter assays using HEK293T cells
270 co-transfected with miRNA agomir and recombinant pmirGLO vectors containing the predicted
271 binding sites for miR-2, miR-14 and miR-34 in the CDS of *DcAKHR*. (C) Dual-luciferase
272 reporter assays using HEK293T cells co-transfected with miR-34 agomir plus recombinant
273 pmirGLO vectors containing *DcAKHR*-3'UTR or mutated *DcAKHR*-3'UTR. (D) Tissue
274 expression pattern of miR-34 in *C*Las+ female adults at 7 DAE in the head, ovary, fat body,
275 and midgut. (E) Comparison of temporal expression patterns of miR-34 in ovaries of *C*Las-
276 and *C*Las+ females. (F) Effect of miR-34 agomir and antagomir treatments on *Dc*AKHR mRNA
277 expression and protein level in ovaries of *C*Las- and *C*Las+ psyllids after 48 h. (G) Relative
278 expression of miR-34 targeted *DcAKHR in vivo* as demonstrated by an RNA
279 immunoprecipitation assay. Data are shown as mean ± SEM. For B-D, significant differences

280 among the different treatments are indicated by lowercase letters above the bars (one-way
281 ANOVA followed by Tukey's Honestly Significant Difference test at $P < 0.05$). The significant
282 differences between treatment and control are indicated by asterisks in E-G (Student's *t*-test,
283 $^{**}p < 0.01$, $^{***}p < 0.001$).
284

285 **miR34 participates in *D. citri*-*C*Las mutualism in ovaries**

286 To investigate the roles of miR-34 in the interaction between *D. citri* and *C*Las,
287 *C*Las-positive and –negative females were fed with agomir-negative control (NC) or with
288 miR-34 agomir. After feeding with miR-34 agomir, there was a significant accumulation of TAG
289 and a decrease in glycogen levels in the two populations (Figures 5A-B). The size of lipid
290 droplets in the fat bodies of *C*Las-positive psyllids were bigger than those of the control (Figure
291 5C). After treatment with miR-34 agomir, ovarian development of *C*Las-positive psyllids was
292 reduced (Figure 5D). In addition, when *C*Las-negative and *C*Las-positive psyllids were fed with
293 miR-34 agomir, the oviposition period of both psyllid types was shortened, preoviposition
294 period was markedly extended, and fecundity significantly decreased compared with the
295 relevant control groups (Figures 5E-G); these phenotypes mimic those expressed after
296 treatment with ds*DcAKHR*. Moreover, the *C*Las signals and relative titer in *C*Las-positive
297 ovaries were significantly reduced (Figures 5H-I). All the results indicate that miR-34
298 suppresses *DcAKHR* expression and is involved in the mutualistic interaction.

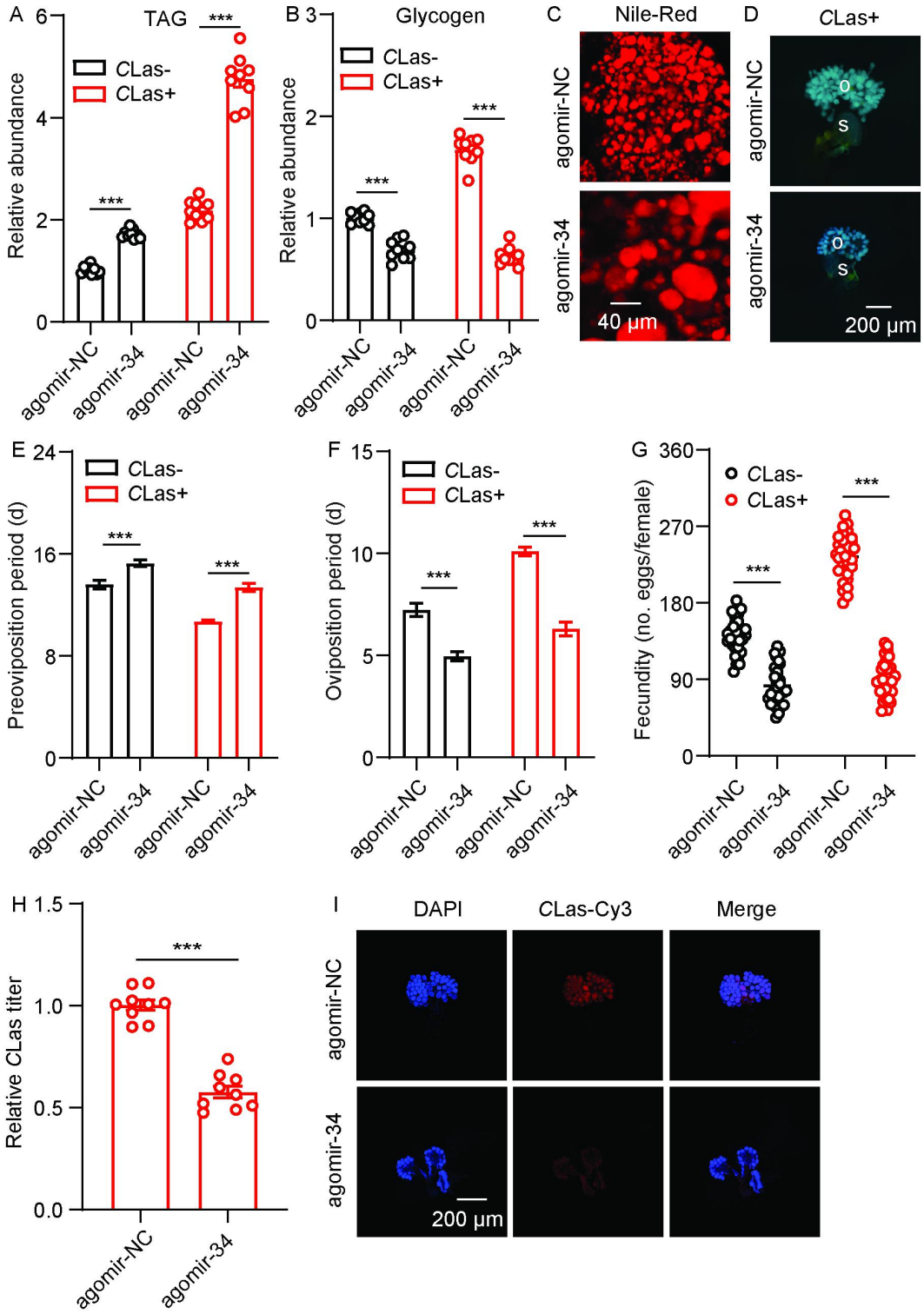

Figure 5. miR-34 participation in mutualistic interactions between *D. citri* and *C*Las. (A) Comparison of TAG levels in fat bodies of *C*Las- and *C*Las+ females treated with agomir-34 for 48 h. (B) Comparison of glycogen levels in the fat bodies of *C*Las- and *C*Las+ females treated with agomir-34 for 48 h. (C) Lipid droplets stained with Nile red in fat bodies

304 dissected from *C*Las+ females treated with agomir-34 for 48 h. Scale bar = 40 μm. (D) Ovary
305 phenotypes of *C*Las+ female treated with agomir-34 for 48 h. Scale bar = 200 μm. o: ovary, s:
306 spermathecae. (E-G) Comparison of the preoviposition period, oviposition period and the
307 fecundity between *C*Las- and *C*Las+ adults treated with agomir-34. (H) *C*Las titer in ovaries of
308 *C*Las+ females treated with agomir-34 for 48 h. (I) Representative confocal images of *C*Las in
309 the reproductive system of *C*Las+ females treated with agomir-34 for 48 h. Scale bar = 200 μm.
310 The signals of DAPI and *C*Las-Cy3 are same as described in Figure 2. Data are shown as
311 means ± SEM. The significant differences between treatment and controls are indicated by
312 asterisks (Student's *t*-test, ***$p < 0.001$).
313
314 **The JH signaling pathway is regulated by the AKH pathway and is involved in the**
315 **increase in fecundity induced by *C*Las**
316 To evaluate whether the JH signaling pathway is regulated by the AKH signaling pathway,
317 we assayed the relative JH titers and the expression levels of several JH pathway-related
318 genes in *DcAKH*-deficient, *C*Las-positive females. Compared to control females, the relative
319 JH titer in the abdomen decreased significantly after *dsDcAKH* treatment for 48 h (Figure 6A).
320 After feeding with *dsDcAKH* for 48 h, the expression levels of the JH receptor gene, *DcMet,*
321 and the downstream transcription factor, *DcKr-h1*, of the JH signaling pathway were
322 significantly reduced in the fat bodies and ovaries (Figures 6B-C). In addition, the expression
323 levels of *DcVg1-like*, *DcVgA1-like* and *DcV*gR, three important downstream genes of the JH
324 signaling pathway related to ovarian development were lower in *DcAKH*-deficient
325 *C*Las-positive females than in controls after dsRNA feeding for 48 h (Figures 6B-C). Similar
326 results were observed in the *DcAKHR*-deficient *C*Las-positive females (Figures 6D-F) as well
327 as *C*Las-positive females fed with agomir-34 (Figures 6G-I). These results suggest that JH
328 signaling pathway is regulated by the AKH-AKHR-miR-34 signaling pathway and is involved in
329 the increased fecundity of *D. citri* induced by *C*Las.

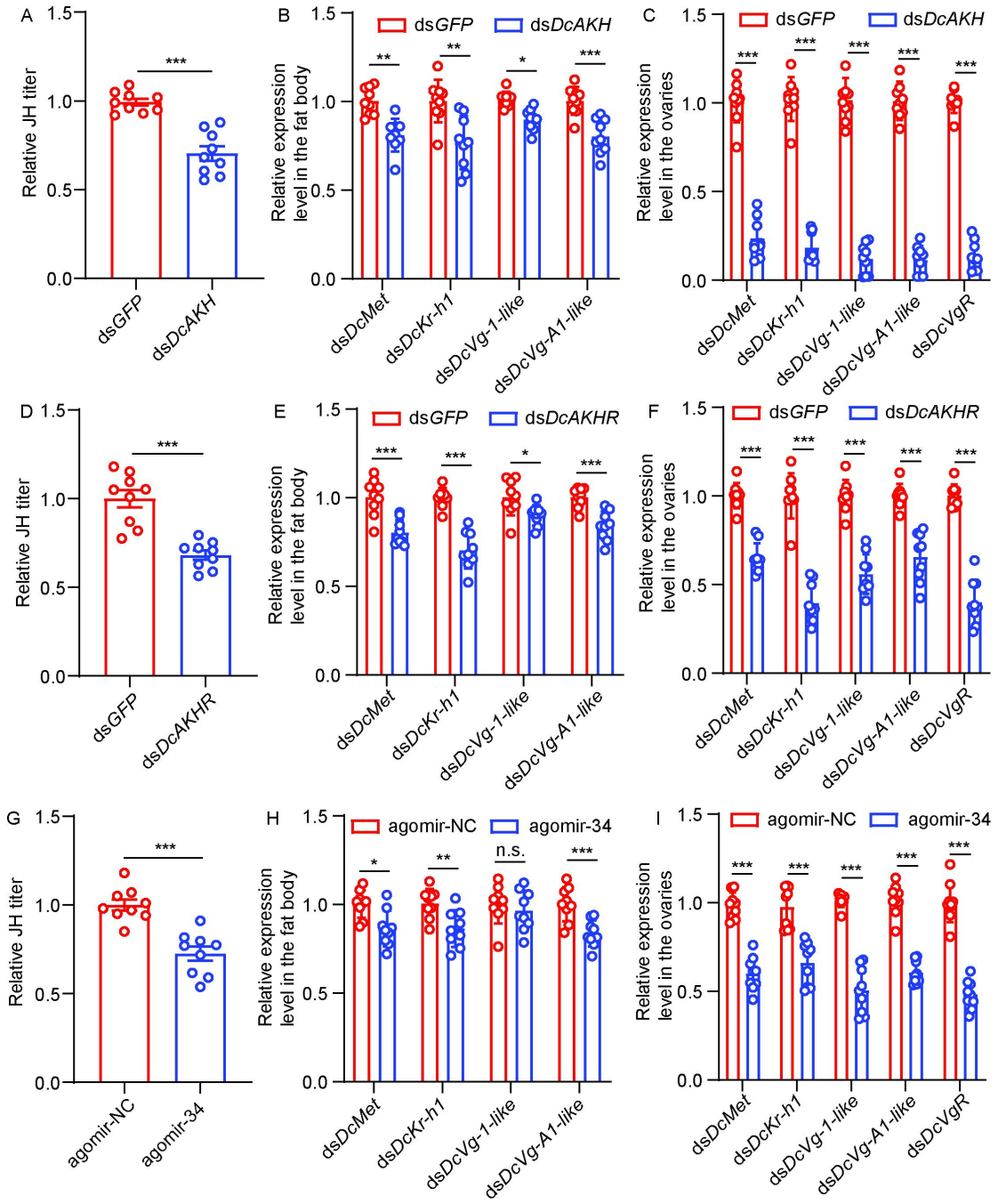

330

331 **Figure 6. The JH signaling pathway is regulated by AKH signaling pathway and is**
332 **involved in the increase in fecundity of *D. citri* induced by *C*Las.** (A) JH titer in the
333 abdomen of *C*Las+ females treated with ds*DcAKH* for 48 h. (B) Effects of ds*DcAKH* treatment
334 on mRNA level of JH signaling pathway in fat bodies of *C*Las+ females. (C) Effects of
335 ds*DcAKH* treatment on mRNA levels of components of the JH signaling pathway in the ovaries
336 of *C*Las+ females. (D) JH titers in the abdomens of *C*las+ females treated with ds*DcAKHR* for
337 48 h. (E) Effects of ds*DcAKHR* treatment on mRNA level of JH signaling pathway in fat bodies
338 of *C*Las+ females. (F) Effects of ds*DcAKHR* treatment on mRNA levels of components of the

339 JH signaling pathway in ovaries of *C*Las+ females. (G) JH titer in abdomen of *C*Las+ females
340 treated with agomir-34 for 48 h. (H) Effects of agomir-34 treatment on mRNA levels of
341 components of the JH signaling pathway in fat bodies of *C*Las+ females. (I) Effects of
342 agomir-34 treatment on mRNA levels of components of the JH signaling pathway in the
343 ovaries of *C*Las+ females.
344

Discussion

An increasing number of studies have focused on the effects of vector-virus interactions on reproduction. For example, rice gall dwarf virus is transmitted vertically by hitchhiking on insect sperm, thereby promoting long-term viral epidemics and persistence in nature [2]. Berasategui et al. (2022) [3] found a mutualistic relationship between *Chelymorpha alternans* and *Fusarium oxysporum*, where the pupae were protected in exchange for the dissemination and propagation of the fungus. Although there is limited research on the mechanisms underlying vector-bacteria interactions. In *D. citri*-*C*Las interaction, *C*Las operates host hormone signaling and miRNA to mediate the mutualistic interactio between *D. citri* fecundity and its replication [35]. Singh and Linksvayer (2020) [41] found that *Wolbachia*-infected colonies of *Monomorium pharaonis* exhibited increased colony-level growth, accelerated colony reproduction, and shortened colony life cycles compared to uninfected colonies.

The fat body is the major insect storage organ that produces the majority of hemolymph-born vitellogenic proteins and critically contributes to insect ovary development [16]. In this study, after infection with *C*Las, the preoviposition period of *D. citri* was shortened, oviposition period was prolonged, and fecundity was significantly increased. These results suggests that there is a mutualistic interaction in *D. citri* ovaries with *C*Las. *C*Las accelerates ovarian development and prolongs the oviposition period thereby enhancing the fecundity of *D. citri*; in turn, *D. citri* provides sites and nutrients for *C*Las replication during ovarian development. *C*Las-positive *D. citri* require more energy to support this increased fecundity. Hence, the TAG and glycogen levels of both *C*Las-positive and *C*Las-negative were assayed. After infection with *C*Las, the TAG and glycogen levels significantly increased, and the average size of lipid droplets in the fat bodies were distinctly larger, indicating that the increase in lipid mobilization may prepare for an increase in fecundity.

The total amount of lipids present in fat bodies is a balance between lipogenesis and lipolysis [42], and both processes are essential for lipid homeostasis. Disruption of either lipogenesis or lipolysis could interfere with nutritional and physiological conditions in fat bodies and affect vitellogenesis. AKH/AKHR mediated lipolytic systems are essential for lipid provision and nutrient transfer during reproduction. In *Gryllus bimaculatus* [43,44] and *Caenorhabditis elegans* [45], injections of AKH interfered with egg production by inhibiting the

375 production of vitellogenins and the accumulation of lipid stores. In *Bactrocera dorsalis*, AKHR
376 knockdown led to decreased lipolytic activity and delayed oocyte maturation [29] and these
377 authors suggested the decline in fecundity may be due to the inability to utilize the lipid stores
378 of fat bodies to promote oocyte maturation. In *Glossina morsitans*, the silencing of *AKHR* and
379 *brummer* led to the inability to mobilize lipid reserves in fat bodies during pregnancy, slowed
380 down the development of oocytes, and caused embryogenesis to fail, indicating that female
381 fertility depends on lipid metabolism regulated by AKHR [24]. These results suggest that lipid
382 homeostasis appears critical for insect fecundity, as its disruption substantially suppresses
383 egg production and negatively affects vitellogenesis.

384 In the study, *DcAKH* and *DcAKHR* played important roles in the increased lipid
385 metabolism and fecundity of *D. citri* mediated by *C*Las. The cDNA sequences encoding AKH
386 and AKHR from *D. citri* were cloned and identified, and phylogenetic analysis showed that
387 *DcAKH* and *DcAKHR* were orthologous to other hemipteran AKHs and AKHRs. Functional
388 analysis showed that *DcAKHR* shares properties found with other AKHRs.
389 *DcAKHR*-transfected CHO cells could be activated by AKH peptide, while it did not response
390 to Crz peptide, despite the sequences and gene structures of AKH and Crz being closely
391 related [21]. *DcAKH* and *DcAKHR* were more highly expressed in the ovaries of *C*Las-positive
392 psyllids than those of *C*Las-negative individuals. Knockdown of *DcAKH* and *DcAKHR* resulted
393 in TAG accumulation and a significant decrease in glycogen levels in the fat bodies. Most
394 importantly, the *C*Las titer in the ovaries of *C*Las-positive psyllids and fecundity significantly
395 reduced when feeding with *dsDcAKH* and *dsDcAKHR*. Our results support the idea that
396 reproductive disruption from AKH/AKHR knockdown is due to the inability of female to mobilize
397 lipid reserves in the fat bodies required for oocyte maturation during vitellogenesis.

398 To date, there are no reports on the post-transcriptional regulation of AKHR. As important
399 post-transcriptional regulators, miRNAs generally suppress their target genes by triggering
400 mRNA degradation or translational repression [32]. There is increasing evidence implicating
401 miRNAs in the metabolic processes of insects, particularly in relation to reproduction. In
402 addition to functions of miR-277 described in the Introduction, this miRNA targets ilp7 and ilp8
403 thereby controlling lipid metabolism and reproduction in *A. aegypti* [40]. miR-8 depletion in
404 mosquitoes resulted in an increase of its target gene, *secreted wingless-interacting molecule*,

405 and in lipid accumulation in developing oocytes [46]. Depletion of miR-8 in mosquitoes by
406 antagomir injection upregulates *secreted wingless-interacting molecule* and decreases the
407 level of lipid in ovaries to block vitellogenesis post blood meals [47]. A switch from catabolic to
408 anabolic amino acid metabolism in fat bodies mediated by miR-276 restricts mosquito
409 investment into oogenesis and benefits the development of *Plasmodium falciparum* [48]. In the
410 current study, based on *in vitro* and *in vivo* experiments, we found that host miR-34 targets
411 *DcAKHR*. miR-34 was observed to have an opposite expression trend to *DcAKHR*, and its
412 expression in the ovaries of *C*Las-positive psyllids was lower than in those of CLas-negative
413 individuals. Treatment of miR-34 agomir and antagomir, respectively, resulted in a significant
414 decrease and increase in *DcAKHR* mRNA and protein levels. In addition, miR-34
415 overexpression not only led to the accumulation of TAG and the reduction of glycogen levels in
416 fat bodies, but also decreased fecundity and *C*Las titers in the ovaries similar to the
417 phenotypes caused by silencing of *DcAKHR*. This indicates that *C*Las inhibited host miR-34 to
418 enhance *DcAKHR* expression and improve the lipid metabolism and fecundity. This study is
419 the first to report the manipulation of host miRNAs and target genes by a bacterium to affect
420 lipid metabolism and reproduction of their vector.

421 Vitellogenesis is strongly linked with insect JH production [49]. The fat body is an
422 important tissue that senses and integrates various nutritional and hormonal signals required
423 for the regulation of vitellogenesis [16]. Moreover, JH is also involved in the nutrient-dependent
424 regulation of insect reproduction, but the mechanism of action remains obscure. Lu et al.
425 (2016a, b) [50,51] have demonstrated that nutritional signaling during female reproduction
426 induces JH biosynthesis that in turn stimulates vitellogenin expression in fat bodies and egg
427 production in *N. lugens.* In order to evaluate the possible relationship between
428 AKH/AKHR-mediated lipolysis and JH-dependent vitellogenesis, the expressions of JH
429 signaling pathway-related genes in fat bodies and ovaries were determined after knockdown of
430 *DcAKH* and *DcAKHR*. We found that reducing *DcAKH* or *DcAKHR* by RNAi in *C*Las-positive *D.*
431 *citri* not only decreased JH titer but also resulted in a decrease in the expression of *DcMet* and
432 *DcKr-h1* in the fat bodies and ovaries, as well as the egg development related genes,
433 *DcVg-1-like*, *DcVg-A1-like* and *DcVgR*. Similar results were detected in the agomir-34
434 treatment. Our results suggest that AKH/AKHR-based lipolysis plays an important regulatory

435 role in the JH signaling pathway during *D. citri*-*C*Las interactions.

436 In conclusion, we proposed the scheme of events following *C*Las infection presented in
437 Figure 7. Upon infection with *C*Las, *D. citri* exhibits enhanced fecundity compared to
438 uninfected individuals.The interaction between *C*Las and *D. citri* affecting reproduction is a
439 win-win strategy; the increased offspring of *D. citri* contributes to a higher presence of *C*Las in
440 the field. *C*Las upregulates the AKH/AKHR signaling and downregulates miR-34 to increase
441 lipid metabolism and activate JH-dependent vitellogenesis, thereby improving the fecundity of
442 *C*Las-positive females. Overall, our results not only broaden our understanding of the
443 molecular mechanism underlying the *D. citri*-*C*Las interaction, but also provide valuable
444 insights for further integrated management of *D. citri* and HLB by targeting the
445 *DcAKH/DcAKHR* signaling pathway.
446

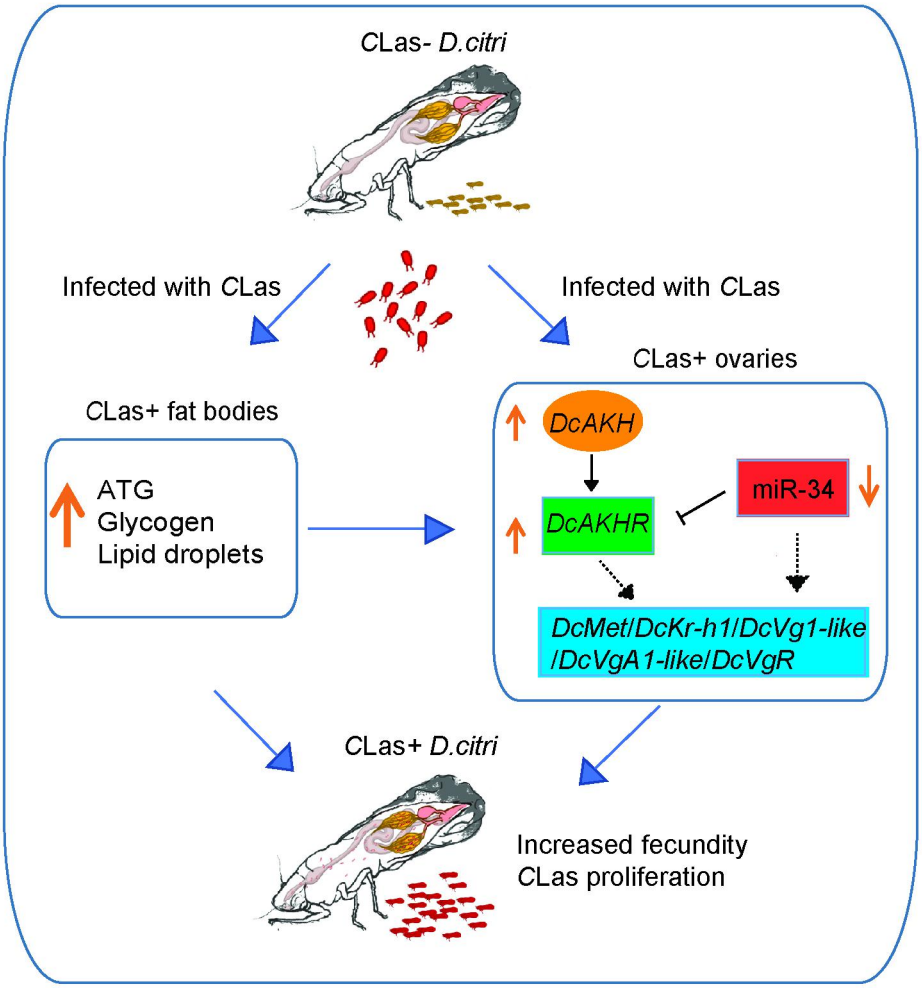

447

448 **Figure 7. Mechanisms linking metabolism and reproduction of *D. citri* induced by CLas.**
449 After infection with CLas, the TAG and glycogen levels in fat bodies of CLas-positive psyllids
450 significantly increased as well as the size of lipid droplets. In ovaries, CLas upregulates the
451 AKH/AKHR signaling and downregulates miR-34 to increase lipid metabolism and activate
452 JH-dependent vitellogenesis, thereby improving the fecundity of CLas-positive females. *D. citri*
453 are more fecund than their uninfected counterparts. The interaction between CLas and *D. citri*
454 affecting reproduction is a win-win strategy; the more offspring of *D. citri*, the more CLas in the
455 field.
456

457 ## Materials and Methods

458 **Host plants and insect colonies**

459 The *C*Las-negative (healthy) and *C*Las-positive *D. citri* colonies were obtained from a
460 laboratory culture continuously reared on the healthy and *C*Las-infected lemon (*Citrus ×limon*
461 (L.) Osbeck) plants. Monthly monitoring of the *C*Las infection in both the lemon plants and
462 psyllids was conducted using quantitative polymerase chain reaction (qPCR). The two
463 populations were raised in different incubators with same conditions (26 ± 1 ℃, 65 ± 5%
464 relative humidity (RH) and a 14-h light: 10-h dark cycle). *C*Las-negative and *C*Las-positive
465 lemon plants were grown in two separate glasshouses.

466

467 **Bioinformatics and phylogenetic analyses**

468 The physicochemical properties of *DcAKH* (GenBank accession number: MG550150.1)
469 and *DcAKHR* (GenBank accession number: OR259432) were analyzed using the online
470 bioinformatics ProtParam tool (http://web.expasy.org/protparam/). Search and download
471 amino acid sequences of other species in the NCBI database. Homologous protein sequences
472 of AKH and AKHR were aligned with those of other insects using DNAman6.0.3 software.
473 Phylogenetic trees were constructed with the neighbor-joining method in MEGA5.10 software,
474 with 1000 bootstrap replicates; bootstrap values > 50% shown on the tree.

475

476 **Assays of reproductive parameters**

477 Tested females from two colonies were selected and paired with healthy males. One
478 female and one male were placed onto young vegetative shoots (flush) of healthy lemon plants
479 to promote oviposition; the flush and insects were sealed with tied white mesh bag (15 × 20
480 cm). These lemon plants were held in an incubator (25 ± 1 ℃, 65 ± 5% RH, 14L: 10D
481 photoperiod). After 24h, the preoviposition period and oviposition period were recorded, the
482 number of eggs laid per female were counted, and this pair of psyllids were transferred to new
483 flush to continue egg laying. Eggs were counted daily until all females died. All the
484 experiments were performed using three replications, and about 15 pairs of *D. citri* for each
485 replication.

486

487 **Quantitative RT-PCR (qRT-PCR)**

488 For mRNA expression analysis, total RNA was extracted using TRIzol reagent (Invitrogen,
489 Carlsbad, CA, United States), and the synthesis of first-strand cDNA was performed using a
490 PrimeScript™ II 1st Strand cDNA Synthesis Kit (Takara, Beijing, China) in accordance with the
491 manufacturer's instructions. qRT-PCR was carried out by using the TB Green® Premix Ex
492 Taq™ II (Takara, Beijing, China) on an ABI PRISM® 7500 Real-Time System (Applied
493 Biosystems, Foster City, CA, USA). The beta-actin (*Dcβ-ACT*, GenBank XM_026823249.1)
494 gene was used as an internal control to normalize gene expression levels. For miRNA
495 expression analysis, miRNA was extracted using a miRcute miRNA Isolation Kit (TIANGEN,
496 Beijing, China), synthesized using a miRcute Plus miRNA First-Strand cDNA Kit (TIANGEN,
497 Beijing, China), and quantified using the miRcute Plus miRNA qPCR Kit (SYBR Green)
498 (TIANGEN, Beijing, China). U6 snRNA was used as an internal control to normalize the
499 expression of miRNA. All the primers used are listed in Supplementary Table 1.

500

501 **Luciferase activity assay**

502 The 185 bp sequence of the 3'UTR containing the predicted target sites for miR-34 in
503 *DcAKHR* was cloned into the pmirGLO vector (Promega, Wisconsin, USA) downstream of the
504 luciferase gene to construct the recombinant plasmid, *DcAKHR*-3'UTR-pmirGLO, using the
505 pEASY®-Basic Seamless Cloning and Assembly Kit. The mutated 3'UTR sequence was
506 amplified and cloned into the pmirGLO vector to generate the *DcAKHR*-3'UTR
507 mutant-pmirGLO plasmid. The agomir and antagomir of miRNAs were chemically synthesized
508 and modified by GenePharma (Shanghai, China) with chemically modified RNA oligos of the
509 same sequence or anti-sense oligonucleotides of the miRNA. The negative control for agomir
510 and antagomir was provided by the manufacturer. According to the manufacturer's instructions,
511 the constructed vector (500 ng) and miRNA agomir (275 nM) were co-transferred into
512 HEK293T cells in a 24-well plate using a Calcium Phosphate Cell Transfection Kit (Beyotime,
513 Nanjing, China). After co-transfection for 24 h, the activities of firefly and Renilla luciferase
514 were detected using the Dual-Glo Luciferase Assay System (Promega, Madison, WI, USA),
515 and the average luciferase activity was calculated.

516

517 **Fluorescence in situ hybridization (FISH)**

518 FISH using a *C*Las probe was carried out as previously described [52]. Under a dissecting
519 microscope, the ovaries of *C*Las-negative and *C*Las-postive *D. citri* were dissected in 1 ×
520 phosphate-buffered saline (PBS) (Beyotime Biotechnology, Shanghai, China). Firstly, the
521 isolated ovaries were fixed in Carnoy's fixative (glacial acetic acid-ethanol-chloroform, 1: 3: 6,
522 vol/vol) for 12 h at 25 ℃, washed four times (5 min each time) with 6% H_2O_2 in 80% ethanol
523 and then three times (10-15 min per time) with PBST (1 × PBS: TritonX-100, 99.7: 0.3,
524 (vol/vol)). Secondly, the samples were pre-incubated three times (10 min per time) in
525 hybridization buffer (20 mM Tris-HCl, pH 8.0, 0.9 M NaCl, 30% formamide (vol/vol), 0.01%
526 sodium dodecyl sulfate (wt/wol)) containing 10 pmol/mL of each probe for 24 h at 25 ℃, then
527 washed three times with PBST. Thirdly, nuclei were stained with 0.1 mg/mL of 40,
528 60-diamidino-2-phenylindole (DAPI) (Sigma-Aldrich, St Louis, MO, USA) for 15 min, then
529 washed once with PBST. Finally, the stained ovaries were mounted in mounting medium. The
530 slides were scanned under a Leica TCS-SP8 (Leica Microsystems Exton, PA USA) confocal
531 microscope; excitation lasers emitting at 405 nm and 550 nm were used to detect the DAPI
532 and Cy3 signals, respectively, and sequential scanning was used to avoid the signal overlap of
533 probes. Image processing was completed using Leica LAS-AF software (v2.6.0). Specificity of
534 detection was carried out using without the probe and *C*Las-negative controls. Three FISH
535 tests were performed and at least 20 ovaries were viewed under the microscope to confirm the
536 repeatability. The probe sequences used in the current study are listed in Supplementary
537 Table 1.

538

539 **Western blotting**

540 The total proteins from *D. citri* ovaries were extracted using RIPA protein lysis buffer (50
541 mM Tris pH 7.4, 1% Triton X-100, 150 mM NaCl, 1% sodium deoxycholate and 0.1% SDS)
542 with 1 mM PMSF. Proteins concentrations were quantified using a BCA protein assay kit
543 (Beyotime, Jiangsu, China). Aliquots of 60 μg protein were separated by 12% SDS-PAGE and
544 transferred to polyvinylidene fluoride membranes (Millipore). Subsequently, the membranes
545 were incubated with the primary antibody against *DcAKHR* (1: 1000 dilution, ABclonal
546 Technology Co., Ltd., Wuhan, China) for 12 h at 4 °C and then with the secondary antibody

547 (goat anti-rabbit IgG conjugated with HRP, 1: 10000 dilution) for 2 h at 25 °C. A mouse
548 monoclonal antibody against β-actin (TransGen Biotech, Beijing, China) was used as a control.
549 Immunoreactivity was imaged with the enhanced chemiluminescence with Azure C600
550 multifunctional molecular imaging system.
551
552 **Nile red staining**
553 The fat bodies were dissected from adult females 5 DAE, fixed in 4% paraformaldehyde
554 for 30 min at 25 ℃, and washed twice with 1 × PBS. Lipid droplets were incubated for 30 min
555 within the mixture of Nile red (0.1 μg/μL, Beijing Coolaber Technology Co., Ltd) and DAPI
556 (0.05 μg/μL), and then washed twice with 1 × PBS. The samples were imaged using a laser
557 scanning microscopy (TCS-SP8, Leica Microsystems Exton, PA USA).
558
559 **Determination of TAG levels**
560 TAG levels were measured using a Triglycerides Colorimetric Assay (Cayman) in
561 accordance with the manufacturer's instructions. In short, thirty fat bodies were homogenized
562 in 100 μL of Diluent Assay Reagent. Then 10 μL of supernatant was incubated with Enzyme
563 Mixture solution, the TAG contents from the measurements were normalized to protein levels
564 in the supernatant of the samples determined using a BCA protein assay (Thermo Fisher
565 Scientific). Three independent biological replicates were analyzed for each treatment, and
566 each treatment included three technical replicates.
567
568 **Determination of glycogen levels**
569 Glycogen levels were assayed using a Glycogen Assay Kit (Cayman) in accordance with
570 the manufacturer's instructions. In brief, thirty fat bodies were homogenized in 100 μL of
571 Diluent Assay Reagent, and 10 μL of supernatant was incubated with Enzyme Mixture solution
572 and Developer Mixture. The glycogen levels from the measurements were normalized to
573 protein levels in the supernatant of the sample determined using a BCA protein assay (Thermo
574 Fisher Scientific). Three independent biological replicates were analyzed for each treatment,
575 and each treatment included three technical replicates.
576

577 **dsRNA synthesis and RNAi assay**

578 dsRNAs of *DcAKH* and *DcAKHR* were transcribed by a Transcript Aid T7 High Yield kit
579 (Thermo Scientific, Wilmington, DE, United states) and purified using the GeneJET RNA
580 Purification kit (Thermo Scientific). miRNA agomir, agomir negative control, miRNA antagomir,
581 and antagomir negative control were synthesized in the Shanghai GenePharma Co. Ltd.
582 (Shanghai, China). The RNAi and miRNA treatments were performed by feeding dsRNA or
583 miRNA antagomir/agomir through an artificial diet as described previously [53]. Briefly, twenty
584 females at 7 DAE were placed into a glass cylinder (25 × 75 mm) and sealed with two
585 stretched paramembranes. 200 μL of 20% (w:v) sucrose mixed with dsRNA was placed
586 between two paramembranes for feeding. The final ingestion concentrations of ds*DcAKH* and
587 ds*DcAKHR* were 200 ng/μL and 300 ng/μL, respectively. After feeding with dsRNA for 48 h,
588 the treated females were assayed as follows. The ovaries were dissected or qRT-PCR and
589 western blot analysis. Reproductive parameters including the pre-oviposition period,
590 oviposition period, and fecundity were recorded. *C*Las titers in the ovaries were assayed.
591 Ovary morphologies were observed using a Ultra-Depth Three-Dimensional Microscope
592 (VHX-500). Fat bodies were stained with Nile red. TAG levels and glycogen levels were
593 determined. Green fluorescent protein (GFP) was used as a reporter gene. Feeding ds*GFP*
594 was used as the control when psyllids were fed with dsRNA. All the experiments were
595 performed in three replications, and each replication included 15-20 pairs of *D. citri*.

596

597 **Heterologous expression and calcium mobilization assay**

598 The complete ORF of *DcAKHR* was cloned into the expression vector pcDNA3.1$^+$; cloning
599 was confirmed by sequencing (TSINGKE Bio). Endotoxin-free plasmid DNA of the vector was
600 extracted, and all tested peptides were synthesized by Sangon Biotech (Shanghai, China) at a
601 purity >95 % (see Fig. 1B for peptide structures). Chinese hamster ovary (CHO-WTA11) cells
602 supplemented with Gα16 subunit and aequorin were used [54] and transfected with
603 pcDNA3.1$^+$-*DcAKHR* or empty pcDNA3.1$^+$ (negative control) vectors using Lipofectamine
604 2000 (Thermo Fisher Scientifc, Waltham, MA USA). The calcium mobilization assay was
605 performed with slight modification as described by Gui et al. (2017) [55] and Shi et al. (2017)
606 [56]. In brief, the cells were incubated for 3 h in the dark with coelenterazine h (Promega,

607 Madison, WI, USA) 48 h after the transfection. Then, serial dilutions of peptide ligands (10^{-6} to
608 10^{1} μM) were loaded into opaque 96-well plates. Luminescence was measured over 15 s
609 using a SpectraMax i3x Multi Mode Microplate Reader (Molecular Devices). Medium alone
610 was used as a blank control and 100 μM ATP was served as a positive control. Each
611 experiment was repeated three times.
612
613 **JH titer detection**
614 JH titers were assessed using the Insect JH Ⅲ ELISA kit (Shanghai Enzyme-linked
615 Biotechnology Co., Ltd. Shanghai, China) following the manufacturer's protocol.
616
617 **Statistical analysis**
618 All statistical values are presented as means ± SEM. Statistical analyses were performed
619 by GraphPad Prism 8.0 software. Student's *t*-test was used to determine the pairwise
620 comparisons at the following significance levels (*$p < 0.05$, **$p < 0.01$, ***$p < 0.001$). For
621 multiple comparisons, one-way ANOVA with Tukey's Honest Significant Difference tests used
622 to separate means at $p < 0.05$.
623
624 ## Acknowledgments
625 This research was supported by the National Natural Science Foundation of China, grant
626 number 32102193, and the Open Competition Program of Ten Major Directions of Agricultural
627 Science and Technology Innovation for the 14th Five-Year Plan of Guangdong Province, grant
628 number 2022SDZG07.
629
630 ## Author Contributions
631 Conceptualization: Jiayun Li, Paul Holford, George Andrew Charles Beattie, Yurong He, Yijing
632 Cen, Xiaoge Nian.
633 Data curation: Jiayun Li, Shujie Wu, Jielan He, Xiaoge Nian.
634 Formal analysis: Jiayun Li, Xiaoge Nian, Desen Wang.
635 Funding acquisition: Xiaoge Nian, Yurong He, Yijing Cen.
636 Investigation: Jiayun Li, Shujie Wu, Jielan He, Shijian Tan, Xiaoge Nian.

637 Methodology: Jiayun Li, Paul Holford, George Andrew Charles Beattie, Yurong He, Xiaoge
638 Nian, Yijing Cen.
639 Project administration: Xiaoge Nian, Yijing Cen.
640 Resources: Jiayun Li, Shujie Wu, Jielan He, Xiaoge Nian, Yijing Cen.
641 Software: Jiayun Li, Xiaoge Nian, Desen Wang.
642 Supervision: Yurong He, Yijing Cen.
643 Validation: Jiayun Li, Paul Holford, George Andrew Charles Beattie, Xiaoge Nian.
644 Visualization: Jiayun Li, Paul Holford, George Andrew Charles Beattie, Yurong He, Xiaoge
645 Nian, Yijing Cen.
646 Writing-original draft: Jiayun Li, Xiaoge Nian, Yijing Cen.
647 Writing-review & editing: Jiayun Li, Paul Holford, George Andrew Charles Beattie, Xiaoge Nian,
648 Yijing Cen.
649

650 ## Competing interests

651 The authors declare no conflict of interest.
652

653 ## Data Availability Statement

654 The published article includes all data generated or analyzed during this study. The full
655 sequences were submitted to NCBI, accession number: MG550150.1 for *DcAKH*, OR259432
656 for *DcAKHR*, OP251123 for *DcMet*, XM_026820026.1 for *DcKr-h1*, XM_008488883.3 for
657 *DcVg-1-like*, XM_026832896.1 for *DcVg-A1-like* and OP251122 for *DcVgR*.
658

659 ## References

660 [1] Eigenbrode SD, Bosque-Pérez NA, Davis TS. Insect-borne plant pathogens and their
661 vectors: Ecology, evolution, and complex interactions. Annu Rev Entomol. 2018;
662 63:169-191.
663 [2] Mao QZ, Wu Wei, Liao ZF, Li JJ, Jia DS, Zhang XF, et al. Viral pathogens hitchhike with
664 insect sperm for paternal transmission. Nat Commun. 2019; 10:955.
665 [3] Berasategui A, Breitenbach N, García-Lozano M, Pons I, Sailer B, Lanz C, et al. The leaf
666 beetle *Chelymorpha alternans* propagates a plant pathogen in exchange for pupal

667 protection. Curr Biol. 2022; 32:4114-4127.
668 [4] Ray S, Casteel CL. Effector-mediated plant-virus-vector interactions. Plant Cell. 2022;
669 34:1514-1531.
670 [5] Capoor SP, Rao DG, Viswanath SM. *Diaphorina citri* Kuwayama. A vector of the greening
671 disease of citrus in India. Indian J. Agric. Sci, 1967; 37:572-576.
672 [6] Gottwald TR. Current epidemiological understanding of citrus Huanglongbing. Annu Rev
673 Phytopathol. 2010; 48:119-139.
674 [7] Bové JM. Huanglongbing or yellow shoot, a disease of Gondwanan origin: Will it destroy
675 citrus worldwide? Phytoparasitica. 2014; 42:579-583.
676 [8] da Graça JV, Douhan GW, Halbert SE, Keremane ML, Lee RF, Vidalakis G, et al.
677 Huanglongbing: An overview of a complex pathosystem ravaging the world's citrus. J
678 Integr Plant Biol. 2016; 58:373-387.
679 [9] Fuentes A, Braswell WE, Ruiz-Arce R, Racelis A. Genetic variation and population
680 structure of *Diaphorina citri* using cytochrome oxidase I sequencing. PLoS ONE. 2018;
681 13:e0198399.
682 [10] Beattie GAC. Management of the Asian citrus psyllid in Asia. In: Qureshi JA, Stansly PA
683 (eds) Asian citrus psyllid: biology, ecology and management of the huanglongbing vector.
684 CAB International, Wallingford, UK. 2020; 179-209.
685 [11] Graham J, Gottwald T, Setamou M. Status of huanglongbing (HLB) outbreaks in Florida,
686 California and Texas. Tropical Plant Pathology. 2020; 45:265-278.
687 [12] Li S, Wu F, Duan Y, Singerman A, Guan Z. Citrus greening: Management strategies and
688 their economic impact. HortScience. 2020; 55:604-612.
689 [13] Pelz-Stelinski KS, Killiny N. Better together: Association with '*Candidatus* Liberibacter
690 asiaticus' increases the reproductive fitness of its insect vector, *Diaphorina citri*
691 (Hemiptera: Liviidae). Ann Entomol Soc Am. 2016; 109:371-376.
692 [14] Ren SL, Li YH, Zhou YT, Xu WM, Cuthbertson AGS, Guo YJ et al. Effects of *Candidatus*
693 Liberibacter asiaticus on the fitness of the vector *Diaphorina citri*. J Appl Microbiol. 2016;
694 121:1718-1726.
695 [15] Wu FN, Qureshi JA, Huang JQ, Fox EGP, Deng XL, Wan FH, et al. Host plant-mediated
696 interactions between '*Candidatus* Liberibacter asiaticus' and its vector *Diaphorina citri*

697 Kuwayama (Hemiptera: Liviidae). J Econ Entomol. 2018; 111:2038-2045.
698 [16] Arrese EL, Soulages JL. Insect fat body: energy, metabolism, and regulation. Annu Rev
699 Entomol. 2010; 55:207-225.
700 [17] Stone JV, Mordue W, Batley KE, Morris HR. Structure of locust adipokinetic hormone, a
701 neurohormone that regulates lipid utilisation during flight. Nature. 1976; 263:207-211.
702 [18] Toprak U. The role of peptide hormones in insect lipid metabolism. Front Physiol. 2020;
703 11:434.
704 [19] Azeez OI, Meintjes R, Chamunorwa JP. Fat body, fat pad and adipose tissues in
705 invertebrates and vertebrates: the nexus. Lipids Health Dis. 2014; 13:71.
706 [20] Gáliková M, Diesner M, Klepsatel P, Hehlert P, Xu Y, Bickmeyer I, et al. Energy
707 homeostasis control in *Drosophila* adipokinetic hormone mutants. Genetics. 2015;
708 201:665-683.
709 [21] Park Y, Kim YJ, Adams ME. Identification of G protein-coupled receptors for *Drosophila*
710 PRXamide peptides, CCAP, corazonin, and AKH supports a theory of ligand-receptor
711 coevolution. Proc Natl Acad Sci U S A. 2002; 99:11423-11428.
712 [22] Staubli F, Jorgensen TJ, Cazzamali G, Williamson M, Lenz C, Sondergaard L, et al.
713 Molecular identification of the insect adipokinetic hormone receptors. Proc Natl Acad Sci
714 U S A. 2002; 99:3446-3451.
715 [23] Ziegler R, Isoe J, Moore W, Riehle MA, Wells MA. The putative AKH receptor of the
716 tobacco hornworm, *Manduca sexta*, and its expression. J Insect Sci. 2011; 11:40.
717 [24] Attardo GM, Benoit JB, Michalkova V, Yang G, Roller L, Bohova J, et al. Analysis of
718 lipolysis underlying lactation in the tsetse fly, *Glossina morsitans*. Insect Biochem Mol Biol.
719 2012; 42:360-370.
720 [25] Konuma T, Morooka N, Nagasawa H, Nagata S. Knockdown of the adipokinetic hormone
721 receptor increases feeding frequency in the two-spotted cricket *Gryllus bimaculatus*.
722 Endocrinology. 2012; 153:3111-3122.
723 [26] Jedlička P, Ernst UR, Votavová A, Hanus R, Valterová I. Gene expression dynamics in
724 major endocrine regulatory pathways along the transition from solitary to social life in a
725 bumblebee, *Bombus terrestris*. Front Physiol. 2016; 7:574.
726 [27] Nyasembe VO, Hamerly T, López-Gutiérrez B, Leyte-Vidal AM, Coatsworth H, Dinglasan

727 RR. Adipokinetic hormone signaling in the malaria vector Anopheles gambiae facilitates
728 Plasmodium falciparum sporogony. Commun Biol. 2023; 6(1):171.
729 [28] Karbusová N, Gautam UK, Kodrík D. Effect of natural toxins and adipokinetic hormones
730 on the activity of digestive enzymes in the midgut of the cockroach Periplaneta americana.
731 Arch Insect Biochem Physiol. 2019;101(4):e21586.
732 [29] Hou QL, Chen EH, Jiang HB, Wei DD, Gui SH, Wang JJ, et al. Adipokinetic hormone
733 receptor gene identification and its role in triacylglycerol mobilization and sexual behavior
734 in the oriental fruit fly (*Bactrocera dorsalis*). Insect Biochem Mol Biol. 2017; 90:1-13.
735 [30] Lu K, Wang Y, Chen X, Zhang X, Li W, Cheng Y, et al. Adipokinetic Hormone receptor
736 mediates trehalose homeostasis to promote vitellogenin uptake by oocytes in *Nilaparvata*
737 *lugens*. Front Physiol. 2019; 9:1904.
738 [31] Zheng H, Chen C, Liu C, Song Q, Zhou S. Rhythmic change of adipokinetic hormones
739 diurnally regulates locust vitellogenesis and egg development. Insect Mol Biol. 2020;
740 29:283-292.
741 [32] Bartel DP. Metazoan microRNAs. Cell. 2018; 173:20-51.
742 [33] Asgari S. Role of microRNAs in insect host-microorganism interactions. Front Physiol.
743 2011; 2:48.
744 [34] Asgari S. Role of microRNAs in arbovirus/vector interactions. Viruses. 2014;
745 6:3514-3534.
746 [35] Nian X, Luo Y, He X, Wu S, Li J, Wang D, et al. Infection with '*Candidatus* Liberibacter
747 asiaticus' improves the fecundity of *Diaphorina citri* aiding its proliferation: A win-win
748 strategy. Mol Ecol. 2024; 33:e17214.
749 [36] Zhang SD, An SH, Hoover K, Li Z, Li XR, Liu, XM, et al. Host miRNAs are involved in
750 hormonal regulation of HaSNPV-triggered climbing behaviour in *Helicoverpa armigera*.
751 Mol Ecol. 2018; 27:459-475.
752 [37] Bryant B, Macdonald W, Raikhel AS. microRNA miR-275 is indispensable for blood
753 digestion and egg development in the mosquito *Aedes aegypti*. Proc Natl Acad Sci U S A.
754 2010; 107:22391-22398.
755 [38] Zhang Y, Zhao Bo, Roy S, Saha TT, Kokoza VA, Li M, et al. microRNA-309 targets the
756 Homeobox gene *SIX4* and controls ovarian development in the mosquito *Aedes aegypti*.

757 Proc Natl Acad Sci U S A. 2016; 113:E4828-4836.
758 [39] Song JS, Zhou ST. Post-transcriptional regulation of insect metamorphosis and
759 oogenesis. Cell Mol Life Sci. 2020; 77:1893-1909.
760 [40] Ling L, Kokoza VA, Zhang C, Aksoy E, Raikhel AS. MicroRNA-277 targets *insulin-like*
761 *pseptide 7* and *8* to control lipid metabolism and reproduction in *Aedes aegypti*
762 mosquitoes. Proc Natl Acad Sci U S A. 2017; 114:E8017-E8024.
763 [41] Singh R, Linksvayer TA. *Wolbachia*-infected ant colonies have increased reproductive
764 investment and an accelerated life cycle. J Exp Biol. 2020; 223:jeb220079.
765 [42] Grönke S, Mildner A, Fellert S, Tennagels N, Petry S, Müller G, et al. Brummer lipase is
766 an evolutionary conserved fat storage regulator in *Drosophila*. Cell Metab. 2005;
767 1:323-330.
768 [43] Lorenz MW. Adipokinetic hormone inhibits the formation of energy stores and egg
769 production in the cricket *Gryllus bimaculatus*. Comp Biochem Physiol B Biochem Mol Biol.
770 2003; 136:197-206.
771 [44] Lorenz MW, Gäde G. Hormonal regulation of energy metabolism in insects as a driving
772 force for performance. Integr Comp Biol. 2009; 49:380-392.
773 [45] Lindemans M, Liu F, Janssen T, Husson SJ, Mertens I, Gäde G, et al. Adipokinetic
774 hormone signaling through the gonadotropin-releasing hormone receptor modulates
775 egg-laying in *Caenorhabditis elegans*. Proc Natl Acad Sci U S A. 2009; 106:1642-1647.
776 [46] Lucas KJ, Roy S, Ha J, Gervaise AL, Kokoza VA, Raikhel AS. MicroRNA-8 targets the
777 Wingless signaling pathway in the female mosquito fat body to regulate reproductive
778 processes. Proc Natl Acad Sci U S A. 2015; 112:1440-1445.
779 [47] Page RE Jr, Rueppell O, Amdam GV. Genetics of reproduction and regulation of
780 honeybee (*Apis mellifera* L.) social behavior. Annu Rev Genet. 2012; 46:97-119.
781 [48] Lampe L, Jentzsch M, Kierszniowska S, Levashina EA. Metabolic balancing by miR-276
782 shapes the mosquito reproductive cycle and *Plasmodium falciparum* development. Nat
783 Commun. 2019; 10:5634.
784 [49] Roy S, Saha TT, Zou Z, Raikhel AS. Regulatory pathways controlling female insect
785 reproduction. Annu Rev Entomol. 2018; 63:489-511.
786 [50] Lu K, Chen X, Liu WT, Zhang XY, Chen MX, Zhou Q. Nutritional signaling regulates

787 vitellogenin synthesis and egg development through juvenile hormone in *Nilaparvata*
788 *lugens* (Stål). Int J Mol Sci. 2016; 17:269.
789 [51] Lu K, Chen X, Liu WT, Zhou Q. TOR pathway-mediated juvenile hormone synthesis
790 regulates nutrient-dependent female reproduction in *Nilaparvata lugens* (Stål). Int J Mol
791 Sci. 2016; 17:438.
792 [52] Hosseinzadeh S, Shams-Bakhsh M, Mann M, Fattah-Hosseini S, Bagheri A, Mehrabadi
793 M, et al. Distribution and variation of bacterial endosymbiont and "*Candidatus*
794 Liberibacter asiaticus" titer in the Huanglongbing insect vector, *Diaphorina citri*
795 Kuwayama. Microb Ecol. 2019; 78:206-222.
796 [53] Yu XD, Killiny N. RNA interference of two glutathione S-transferase genes, *Diaphorina*
797 *citri DcGSTe2* and *DcGSTd1*, increases the susceptibility of Asian citrus psyllid
798 (Hemiptera: Liviidae) to the pesticides fenpropathrin and thiamethoxam. Pest Manag Sci.
799 2018; 74:638-647.
800 [54] Jiang HB, Gui SH, Xu L, Pei YX, Smagghe G, Wang JJ. The short neuropeptide F
801 modulates olfactory sensitivity of *Bactrocera dorsalis* upon starvation. J Insect Physiol.
802 2017; 99:78-85.
803 [55] Gui SH, Jiang HB, Liu XQ, Xu L, Wang JJ. Molecular characterizations of natalisin and its
804 roles in modulating mating in the oriental fruit fly, *Bactrocera dorsalis* (Hendel). Insect Mol
805 Biol. 2017; 26:103-112.
806 [56] Shi Y, Jiang HB, Gui SH, Liu XQ, Pei YX, Xu L, et al. Ecdysis triggering hormone
807 signaling (ETH/ETHR-A) is required for the larva-larva ecdysis in *Bactrocera dorsalis*
808 (Diptera: Tephritidae). Front Physiol. 2017; 8:587.

809 Supplemental Information

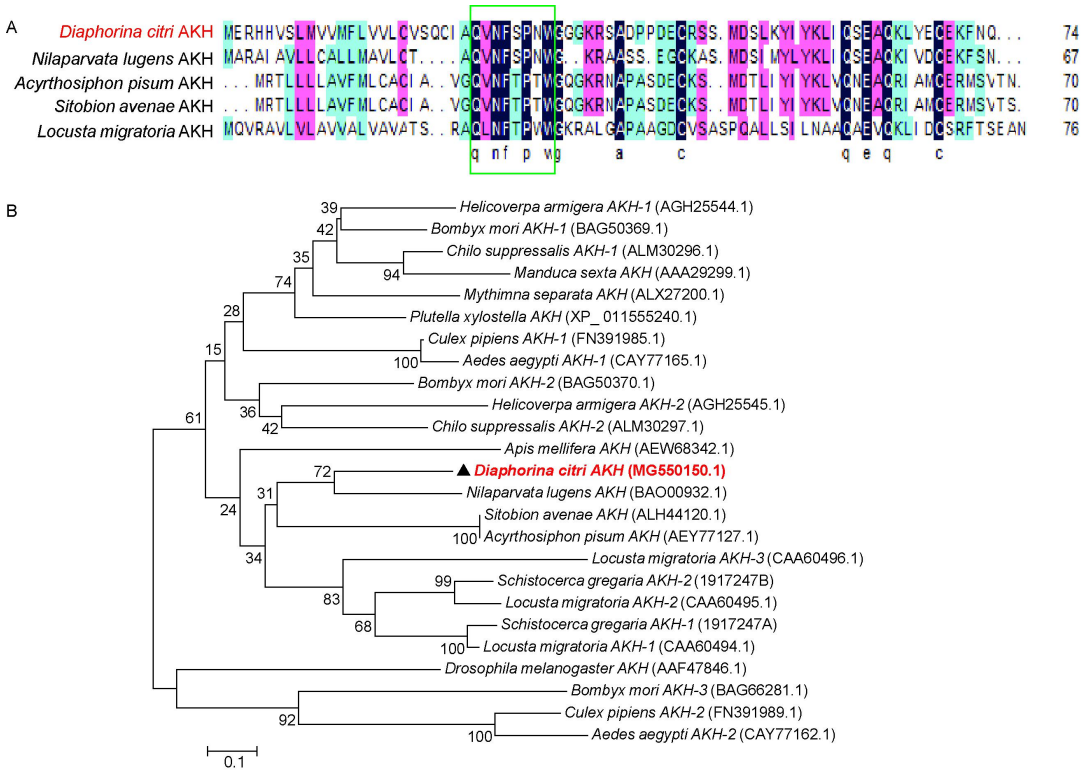

810

811 **Figure S1. Sequence characterization of AKH from different insect species (data are**
812 **related to Figure 2).** (A) Alignment of the amino acid sequences of the *Dc*AKH
813 transmembrane domain with homologs from other insect species. The sequences in the green
814 box represent the mature peptides (QVNFSPNW). (B) Phylogenetic analysis of *Dc*AKH and its
815 homologs in other insect species. The phylogenetic tree was constructed using
816 neighbor-joining with 1000 bootstrap replicates; values > 50% are shown on the tree. The
817 scale bar indicates the number of amino acid substitutions per site.

818

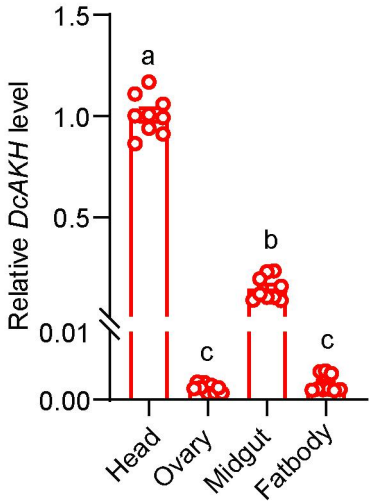

819

820 **Figure S2. Tissue expression of *DcAKH* in *C*Las-positive adult females 9 days after**

821 **emergence in the head, ovary, fat body, and midgut (data are related to Figure 2).**

822

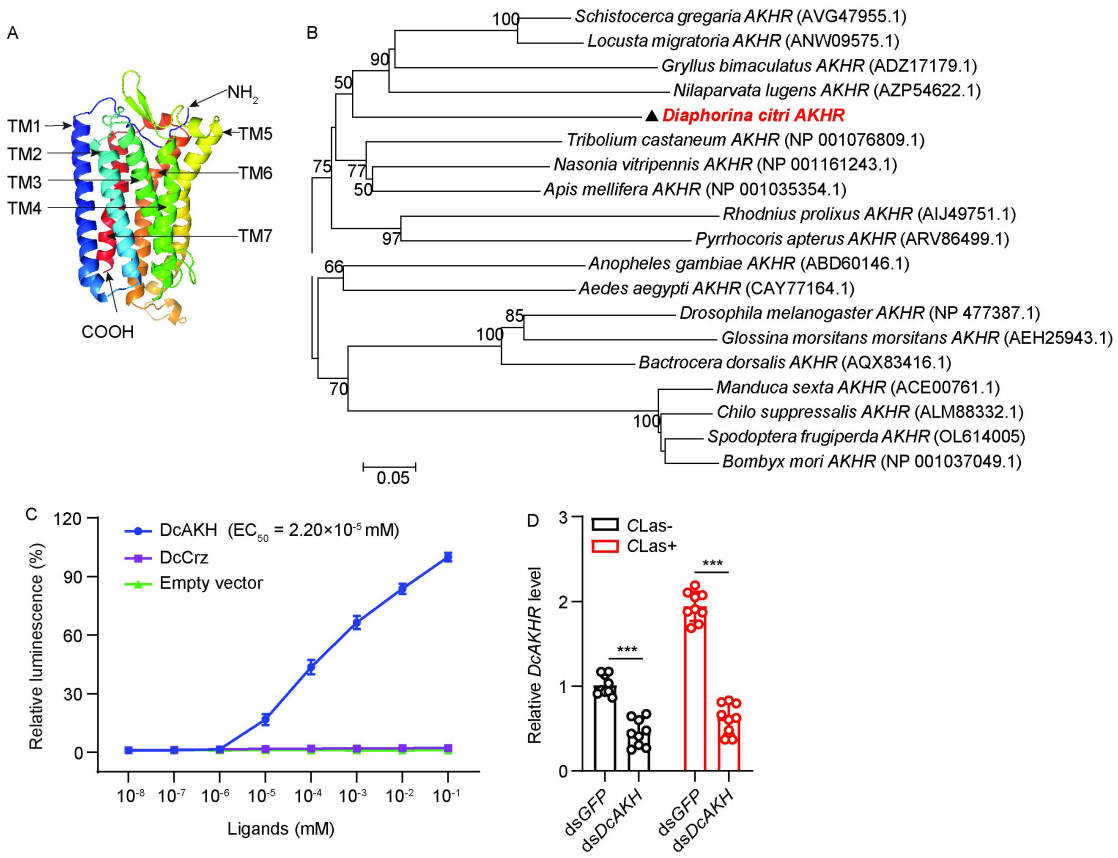

Figure S3. *In vivo* and *in vitro* studies validating the DcAKH-DcAKHR interaction (data are related to Figure 3). The predicted tertiary structure of the *DcAKHR* protein. The seven conserved transmembrane ion channels are shown as TM1-TM7. (B) Phylogenetic analysis the protein sequences of AKHR. The phylogenetic tree was constructed using neighbor-joining with 1000 bootstrap replicates; values > 50% are shown on the tree. The scale bar indicates the number of amino acid substitutions per site. (C) Concentration-response curves for the effect of Ca^{2+} on *DcAKHR*-expression in CHO cells. (D) The expression levels of *DcAKHR* in *C*Las-negative and *C*Las-positive females treated with ds*DcAKH* for 48 h.

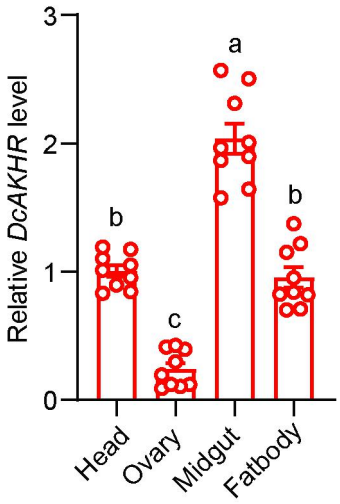

832

833 **Figure S4. Tissue expression of *DcAKHR* in *C*Las-positive female adults 9 DAE in the**

834 **head, ovary, fat body, and midgut (the data are related to Figure 3).**

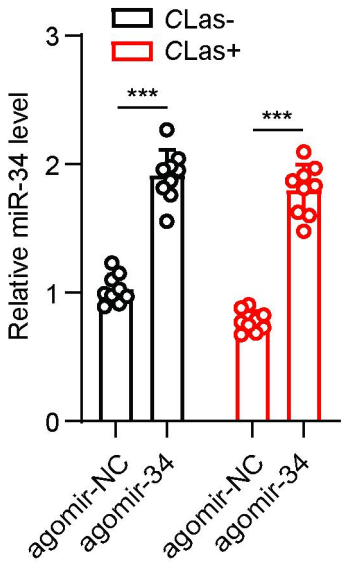

835

836 **Figure S5. The expression levels of miR-34 in *C*Las-negative and *C*Las-positive females**

837 **treated with agomir-34 for 48 h (the data are related to Figure 4).**

838

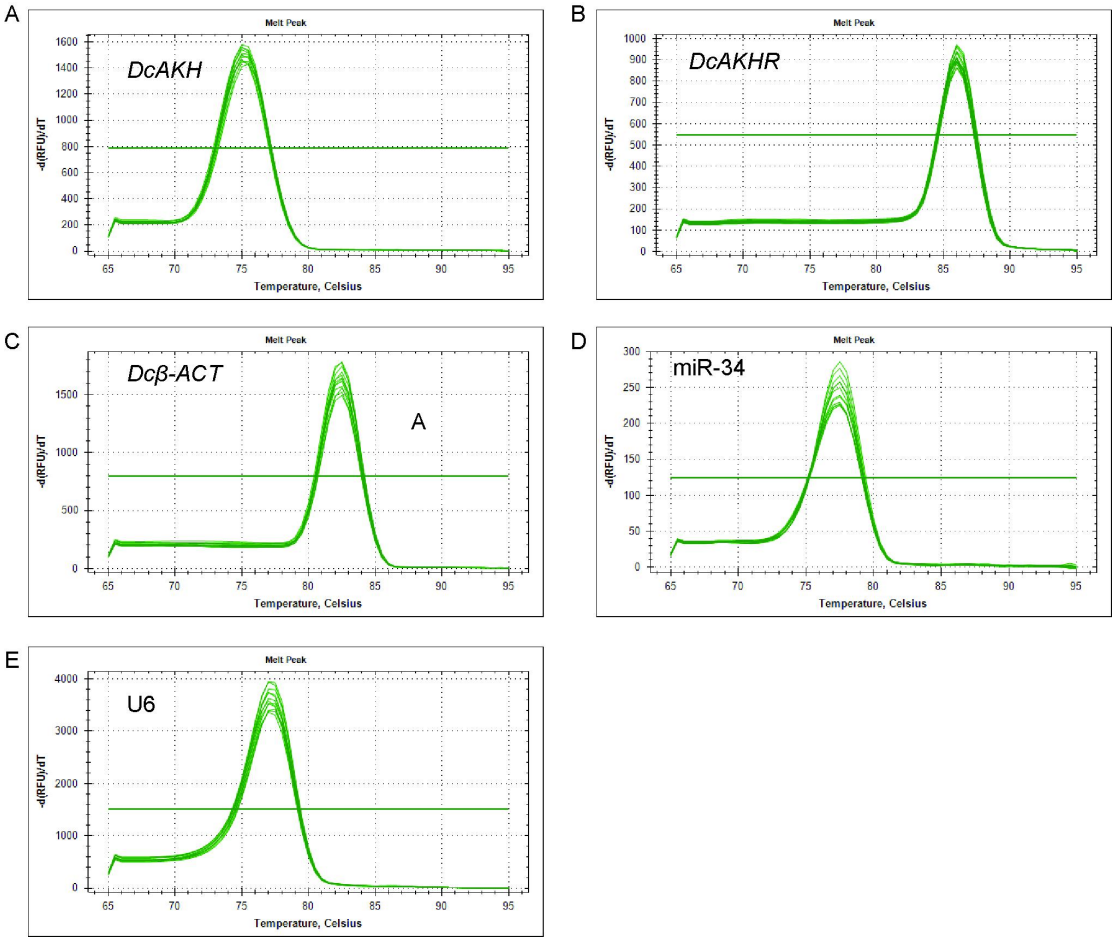

Figure S6. (A-E) Melting curve for qRT-PCR primers of *DcAKH*, *DcAKHR*, *Dcβ-ACT,* miR-34 and U6.

843 **Table S1. Primer list used for 3'RACE, qRT-PCR, and RNAi analysis. Related to Method details.**

Gene name	Accession number	primer name	Sequences of primers (5'-3')	Product size (bp)	Purpose
DcAKH	MG550150.1	*DcAKH*-Full-F	ATGGAGCGACACCATGTGAG	222	Validation of full length sequence
		DcAKH-Full-R	CTGATTGAATTTTTCACATT		
		DcAKH-qF	TGGACTCTCTCAAGTACATTT	54	qRT-PCR
		DcAKH-qR	ACAATTTTTGGGCTTCACTC		
		DcAKH-RNAi-F	taatacgactcactatagggATGGAGCGACACCATGTGAG	138	dsRNA synthesis
		DcAKH-RNAi-R	taatacgactcactatagggGCGACATTCATCAGGAGGAT		
		DcAKH mature peptide	pQVNFSPNW-NH2	-	mature peptide
		DcCrZ mature peptide	pQTFQYSRGWTN-NH2	-	
DcAKHR	OR259432	*DcAKHR*-Full-F	CACATCACCCGGTATGATT	1452	Validation of full length sequence
		DcAKHR-Full-R	CTCCCCAAGATTCAACCTT		
		DcAKHR-3UTR-F	CTGATACGGCCAATAACGTG	185	3'UTR amplification
		3'RACE-Outer Primer	TACCGTCGTTCCACTAGTGATTT		
		DcAKHR-qF	TCAGTTGGAAGAAGGACAAG	116	qRT-PCR
		DcAKHR-qR	GGTACTCAGGCTACACTCTA		

		DcAKHR-RNAi-F	taatacgactcactatagggCTGAGTGGCCTCTGCCTAAC	399	dsRNA synthesis
		DcAKHR-RNAi-R	taatacgactcactatagggTTAACGGCTTCAAAACTGCC		
		DcAKHR-3UTR-Full-F	CTAGTTGTTTAAACGAGCTCTAAGAGAAGAGACTGGCCGG	166	Full sequence of 3'UTR
		DcAKHR-3UTR-Full-R	TGCATGCCTGCAGGTCGACTCTAGACACAGGAGTTTCAATCTATT		
		DcAKHR-3UTR-mutant-F	CTAGTTGTTTAAACGAGCTCGCCACATTGCGTTAAACCGT	166	Mutant sequence of 3'UTR
		DcAKHR-3UTR-mutant-R	TGCATGCCTGCAGGTCGACTCTAGACACAGGAGTTTCAATCTATT		
		DcAKHR-probe	FAM-CACGTTATTGGCCGTATCAG	-	Labled with FAM for FISH
GFP	ACY56286	GFP-RNAi-F	taatacgactcactatagggACTCCAGCAGGACCATGTGATC	596	dsRNA synthesis
		GFP-RNAi-R	taatacgactcactatagggACCTGAAGTTCATCTGCACCAC		
Dcβ-ACT	DQ675553.1	β-ACT-qF	TGTTCCAACCTTCCTTCCTG	109	qRT-PCR
		β-ACT-qR	GTGTTGGCGTACAGGTCCTT		
DcMet	OP251123	*DcMet*-qF	AAGCTCAAGGGCCAAGTCAT	257	qRT-PCR

		DcMet-qR	TAATCAATACCAGGGGCGGC		
DcKr-h1	XM_02682002 6.1	*DcKr-h1-qF*	CTCCAGTGCTGAGTCCACAA	103	qRT-PCR
		DcKr-h1-qR	ATCTCCCGGAGGTTTCTGTT		
DcVg-1-like	XM_0084888 83.3	*DcVg-1-like-qF*	CACCTACTCCTTGTCCTCTA	166	qRT-PCR
		DcVg-1-like-qR	GAAAAATCCCCAGAGTCCTT		
DcVg-A1-like	XM_0268328 96.1	*DcVg-A1-like-qF*	CTCCTCAGAAAGTGGAAGTT	132	qRT-PCR
		DcVg-A1-like-qR	TTGTTTCCGATGAAGTAGGG		
DcVgR	OP251122	*DcVgR-qF*	AGCAGCTGGATATACATGTG	186	qRT-PCR
		DcVgR-qR	CTCCACAGTACTGATTACCG		
*C*Las 16s rRNA	L22532.1	*C*Las 16s-probe	Cy3-CATTATCTTCTCCGGCG	-	Labled with Cy3 for FISH
		*C*Las 16s-qF	TCGAGCGCGTATGCAATACG	-	qRT-PCR
		*C*Las 16s-qR	GCGTTATCCCGTAGAAAAAGGTAG		
miR-34	-	miR34-qF	TGGCAGTGTGGTTAGCTGGTTG		qRT-PCR
		miR-34-probe	Cy3-CACAACCAGCTAACCACACTGCCA	-	Labled with Cy3 for FISH
U6	-	U6-qF	AGGATGACACGCAAAATCGT	-	qRT-PCR

844 Note: The lowercase with underline indicated the T7 promoter sequences in the primers of dsRNA synthesis. The sequences with black boxes displayed the

845 restriction enzyme cutting sites.

846